ELSEVIER

Journal of Fluids and Structures 23 (2007) 983–1011

JOURNAL OF FLUIDS AND STRUCTURES

www.elsevier.com/locate/jfs

Bifurcation analysis and limit cycle oscillation amplitude prediction methods applied to the aeroelastic galloping problem

G.A. Vio, G. Dimitriadis*, J.E. Cooper

School of Mechanical, Aerospace and Civil Engineering, Simon Building, The University of Manchester, Oxford Road, Manchester M13 9PL, UK

Received 7 February 2006; accepted 21 March 2007

Abstract

A global stability and bifurcation analysis of the transverse galloping of a square section beam in a normal steady flow has been implemented. The model is an ordinary differential equation with polynomial damping nonlinearity. Six methods are used to predict bifurcation, the amplitudes and periods of the ensuing Limit Cycle Oscillations: (i) Cell Mapping, (ii) Harmonic Balance, (iii) Higher Order Harmonic Balance, (iv) Centre Manifold linearization, (v) Normal Form and (vi) numerical continuation. The resulting stability predictions are compared with each other and with results obtained from numerical integration. The advantages and disadvantages of each technique are discussed. It is shown that, despite the simplicity of the system, only two of the methods succeed in predicting its full response spectrum. These are Higher Order Harmonic Balance and numerical continuation.

Keywords: Galloping; Aeroelasticity; Harmonic Balance; Normal Form; Numerical continuation; Cell Mapping; Centre Manifold

1. Introduction

Over the last two decades the aeroelastic research community has significantly increased its interest in nonlinear aeroelastic problems. The theoretical research has concentrated on two main areas: (i) full unsteady coupled Computational Fluid Dynamic-Finite Element (CFD-FE) solutions of realistic (or at least reasonably complex) aeroelastic problems; (ii) fundamental solutions of simple nonlinear aeroelastic problems.

The research concerning full unsteady CFD-FE simulations of complex aeroelastic systems is exemplified by Girodroux-Lavigne and Dugeai (2003), Badcock et al. (2005), Garcia (2005) and others. Due to the enormous computational cost of such solutions, the work has mainly concentrated on just obtaining system responses. Additionally, some attempts at predicting the occurrence of bifurcations have been successful Woodgate et al. (2005). Although of limited practicality, fundamental investigations of simple aeroelastic systems have progressed much further in terms of stability prediction, bifurcation analysis and low cost approximate solutions.

*Corresponding author. Tel.: +44 161 2754411; fax: +44 161 2753844
E-mail address: grigorios.dimitriadis@manchester.ac.uk (G. Dimitriadis).

0889-9746/$ - see front matter © 2007 Elsevier Ltd. All rights reserved.
doi:10.1016/j.jfluidstructs.2007.03.006

There are numerous examples of fundamental solutions to nonlinear aeroelastic problems, starting in the 1980s [e.g. Yang and Zhao (1988)] and continuing steadily to the present. The main objectives are usually the prediction of the stability of such aeroelastic systems at a range of flight conditions and of the amplitudes and frequencies of the Limit Cycle Oscillation (LCO) that may be encountered. A typical system investigated by many authors is the pitch-plunge airfoil with various types of nonlinearity. The most popular nonlinearities investigated are cubic stiffness [e.g. Price et al. (1995), Lee et al. (2005) and many others], piecewise-linear stiffness [e.g. Lee (1986) and Conner et al. (1997)] and, more recently, nonlinear aerodynamics [e.g. Thomas et al. (2004), Kholodar et al. (2004), Attar et al. (2005) and Kim et al. (2005)]. Other types of nonlinearities have been investigated such as nonlinearities in the control system (Dimitriadis and Cooper, 2000), due to external stores (Nam et al., 2001) and due to large deformations (Patil et al., 2001).

Bifurcation analysis for simple aeroelastic systems has been performed using numerous methods. These include Cell Mapping (Ding et al., 2005), Harmonic Balance (Yang and Zhao, 1988), Higher Order Harmonic Balance (HOHB) (Raghothama and Narayanan, 1999; Liu, 2005), Centre Manifold (Liu et al., 1999), Normal Form (Vio and Cooper, 2005), numerical continuation (Roberts et al., 2002; Dimitriadis et al., 2005) and others. While these methods have shown various degrees of promise, as yet, there has been no effort to compare their performance and to determine which are the most suitable approaches for aeroelastic problems.

In this paper, a number of bifurcation analysis techniques will be applied to a simple but highly nonlinear aeroelastic system, the aeroelastic galloping problem. These methods are:

(i) Cell Mapping (Hsu, 1987).
(ii) Harmonic Balance (Yang and Zhao, 1988).
(iii) HOHB (Tamura et al., 1981).
(iv) Centre Manifold (Verhulst, 1996).
(v) Normal Form (Leung and Qichang, 1998).
(vi) Numerical continuation (Allgower and Georg, 1990).

The stability predictions obtained from these methods will be compared to results obtained from numerical integration of the equation of motion. Thus, an indication of the effectiveness of such methods can be obtained. The aeroelastic galloping equation has been chosen for this comparison due to its simplicity and ease of application.

2. Aeroelastic galloping

The phenomenon generally called galloping is characterized by structural cross-sections that are aerodynamically unstable, so that small amplitude vibrations generate forces which increase the amplitudes to large values. Galloping is defined as an instability typical of slender structures (Simiu and Scanlan, 1996). It is a relatively low-frequency oscillatory phenomenon of elongated, bluff bodies acted upon by a wind stream. The frequency at which the bluff object responds is much lower than the frequency of vortex shedding. There are two types of galloping: wake and cross-wind (Scruton, 1960).

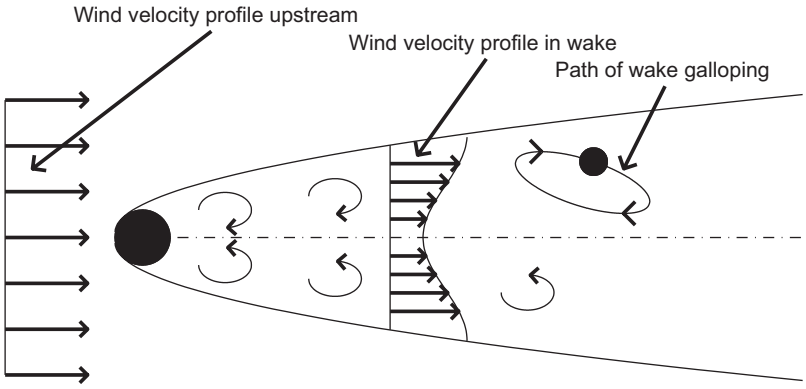

Fig. 1. Wake galloping model.

Wake galloping occurs when two cylinders are present, where one is upstream, producing a wake, and one downstream, within that wake, and the cylinders are separated by a distance of few diameters (Fig. 1). In this type of flow the downstream body is subjected to galloping oscillations induced by the wake of the upstream cylinder. Consequently, the upstream cylinder tends to rotate clockwise while the downstream cylinder rotates anti-clockwise, inducing torsional oscillations (Dowell, 2004). Another type of galloping phenomenon is cross-wind galloping, which occurs when the bluff body has a significant afterbody, i.e. a portion of the body that lies behind the flow separation point (Parkinson, 1989). In this paper only cross-wind galloping will be considered.

Many researchers (Parkinson and Brooks, 1961; Parkinson and Smith, 1964; Bearman and Luo, 1988; Blevins, 1990) have studied the instability mechanism in the flow over a square cylinder, which gives rise to galloping vibration. The quasi-steady theory was first presented in Parkinson and Brooks (1961) where a fifth order polynomial damping nonlinearity was introduced to describe the aerodynamic force. This formulation was later developed in Parkinson and Smith (1964) by extending the approximation up to seventh order. This new approximation allows for an accurate representation of the point of inflection, thus making it possible for the hysteretic phenomenon to appear (refer to Section 4.1 for more details). This phenomenon was not observed in the original study by Parkinson and Brooks (1961). The relationship between point of inflection and the existence of a hysteretic loop was proven by Luo et al. (2003). In Norberg (1993) a dependency between Reynolds number and hysteresis was found experimentally. The validity of quasi-steady theory was investigated in Bearman and Luo (1987, 1988) at different damping levels and reduced frequencies. It is important to note that, for bluff bodies at low reduced velocity, both galloping and vortex-induced vibration can occur. It was concluded that quasi-steady theory is valid as long as the critical reduced velocity is four times the reduced velocity at which vortex resonance occurs. Galloping instability has been the subject of very little research using numerical simulation.

Galloping of a square section in an airflow can be modelled mathematically as a two-dimensional problem, resulting in a single degree of freedom equation of motion with polynomial damping nonlinearity. In a mathematical sense, this nonlinearity can cause LCO. Thus galloping can be described mathematically as an LCO phenomenon.

3. Mathematical model

The aeroelastic galloping problem can be modelled as a mass with linear stiffness and nonlinear damping as shown in Fig. 2. The model is a prism of length l, mass m, square cross-section of height h and is suspended from a linear spring of stiffness k and a linear damper with a damping coefficient of c. The aerodynamic force provides the nonlinear damping, as follows:

$$mx'' + cx' + kx = \tfrac{1}{2}\rho U^2 C_F(\tau) hl, \tag{1}$$

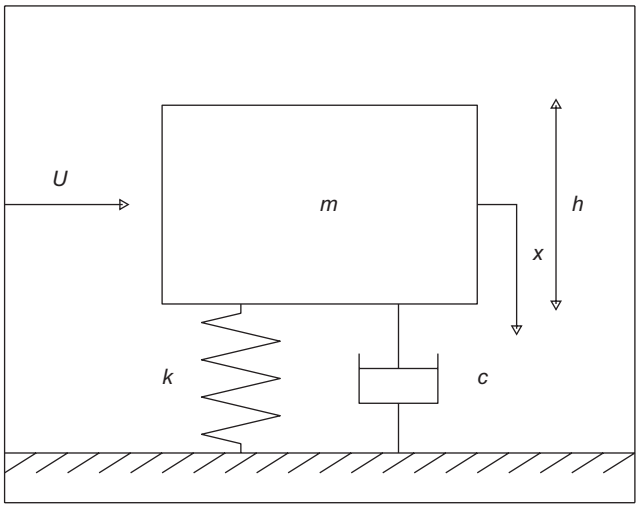

Fig. 2. Aeroelastic galloping model.

where ρ is the air density, U is the airspeed, $(')$ denotes differentiation with respect to time, τ, and the aerodynamic force coefficient, $C_F(\tau)$, is expressed as a polynomial function of velocity, i.e.

$$C_F = A\frac{x'}{U} - B\left(\frac{x'}{U}\right)^3 + C\left(\frac{x'}{U}\right)^5 - D\left(\frac{x'}{U}\right)^7. \tag{2}$$

In this expression $A = 2.69$, $B = 168$, $C = 6270$ and $D = 59\,900$ were obtained empirically by Parkinson and Smith (1964) through curvefitting experimental results. After nondimensionalizing, Eq. (1) becomes

$$\ddot{y} + y = nA\left[\left(V - \frac{2\beta}{nA}\right)\dot{y} - \left(\frac{B}{AV}\right)\dot{y}^3 + \left(\frac{C}{AV^3}\right)\dot{y}^5 - \left(\frac{D}{AV^5}\right)\dot{y}^7\right], \tag{3}$$

where $y = x/h$, $n = \rho h^2 l/(2m)$, V is the nondimensional airspeed given by $V = U/(\omega h)$, $\beta = c/(2m\omega)$, $\omega = \sqrt{k/m}$ and $(\dot{})$ denotes differentiation with respect to the nondimensional time $t = \omega\tau$. This is the full aeroelastic galloping equation of motion, which can be written in compact form as

$$\ddot{y} + y = f(\dot{y}), \tag{4}$$

where

$$f(\dot{y}) = nA\left[\left(V - \frac{2\beta}{nA}\right)\dot{y} - \left(\frac{B}{AV}\right)\dot{y}^3 + \left(\frac{C}{AV^3}\right)\dot{y}^5 - \left(\frac{D}{AV^5}\right)\dot{y}^7\right]. \tag{5}$$

In this study two cases will be considered, as follows.

(a) *Case 1*: Low damping. $\beta = 1.07 \times 10^{-3}$ yields a critical velocity $V_c = 1.85$. This value of β was used in an experimental investigation by Parkinson and Smith (1964).
(b) *Case 2*: High damping. $\beta = 0.5$, which corresponds to $c = m\omega$, yields a critical velocity $V_c = 864.53$.

The critical velocity is obtained by equating the linear damping term in Eq. (3) to zero:

$$V_c = \frac{2\beta}{nA}. \tag{6}$$

The response of the system at nondimensional airspeeds below V_c is decaying. At supercritical speeds the system undergoes LCOs with amplitudes that depend on airspeed and initial conditions.

4. Stability prediction methods

4.1. Numerical integration

Numerical integration of the galloping equation of motion (3) is used to provide the benchmark results to which results from all the other methods will be compared. A number of methods exist for integrating such equations of motion. For this work the Matlab and Simulink ODE suite is used, specifically the ODE45 routine which is based on an explicit Runge–Kutta ((4), (5)) formula, the Dormand–Prince pair (Dormand and Prince, 1980).

For Case 1, due to the low damping forces acting on the system, the simulation time needs to be very high in order to capture the steady-state response. To produce the response almost 1 000 000 simulation points were used at a time increment Δt of 0.125. The response settles to an LCO after a time index of approximately 10^5. For Case 2, only 250 000 simulation points were needed at a nondimensional time increment of 0.06.

Once the response has settled into an LCO, the amplitude and period of the motion can be estimated. There are various approaches for performing this calculation but, for the galloping problem where the LCOs are always symmetric period-1, the amplitude is obtained from the maximum value of the response, $\max(y(t))$, and the period from the time-lapse between two consecutive zero crossings of $y(t)$ in the positive y direction.

Time response plots obtained by numerical integration are not practical for obtaining a description of the global behaviour of the system. Global results (from many airspeeds and initial conditions) can be presented in the form of bifurcation diagrams. A bifurcation diagram is obtained by plotting the maxima of the steady-state response of the system at each airspeed and for every set of initial conditions (essentially, it is a series of Poincaré plots).

The case of aeroelastic galloping is interesting to study as it presents two coexisting limit cycles within a range of airspeeds, giving rise to an hysteretic loop, as displayed in Fig. 3, which is the bifurcation diagram for Case 1. As the

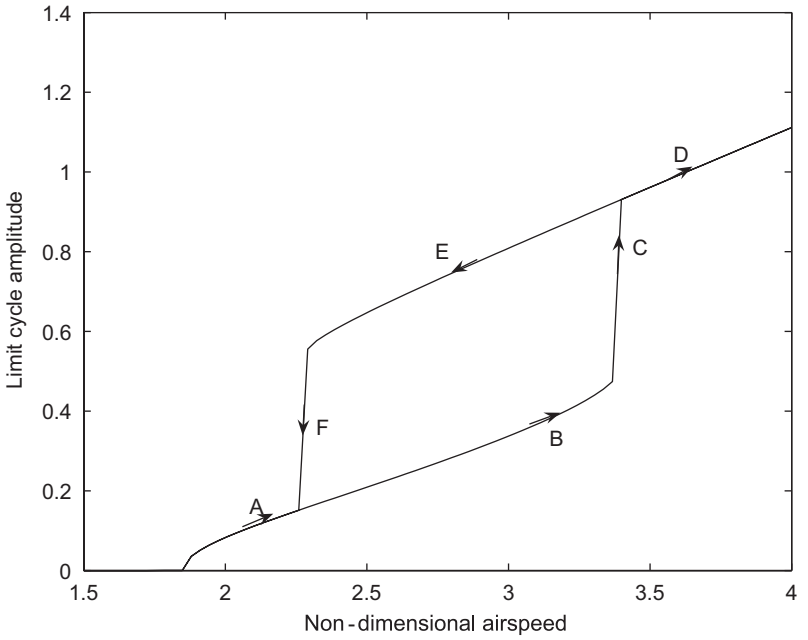

Fig. 3. Hysteretic loop.

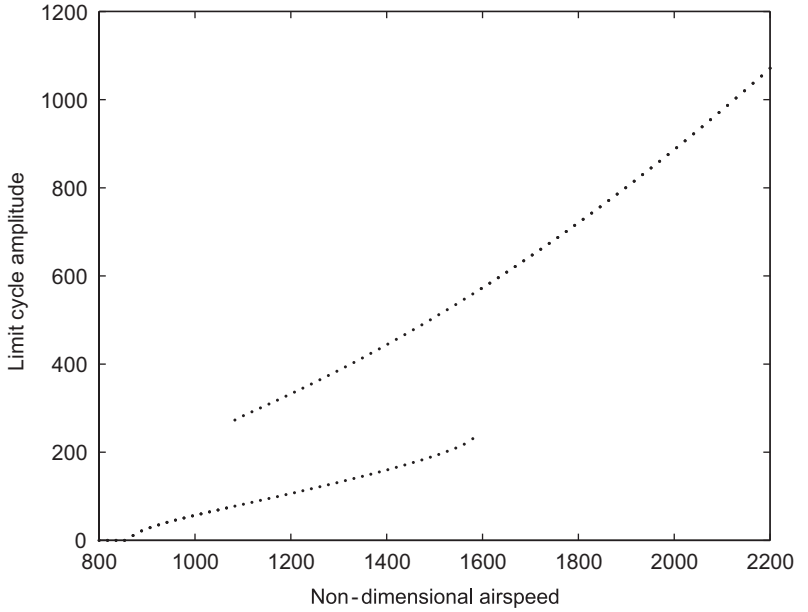

Fig. 4. LCO amplitude using numerical integration for Case 2.

airspeed is increased the LCO amplitude increases from point A to point B, but with a further increase in airspeed it jumps via C to the next stable branch of the bifurcation, moving to point D. If the airspeed is then decreased the response amplitude stays on the upper part of the bifurcation branch via point E but, when the branch becomes unstable the solution jumps to the lower part through F towards A, thus completing the hysteretic loop. The bifurcation

diagram obtained via numerical integration for Case 2 is presented in Fig. 4. To obtain both branches present in the bifurcation plots, multiple simulations at different initial conditions were required.

(i) *Case* 1: For nondimensional airspeeds lower than $V_c = 1.85$ the response of the system is decaying and the limit cycle amplitude is zero. At speeds between 1.85 and 2.4 the system undergoes LCOs with increasing amplitude. At speeds between 2.4 and 3.5 two LCO amplitudes coexist. The system can reach either one of these two LCOs,

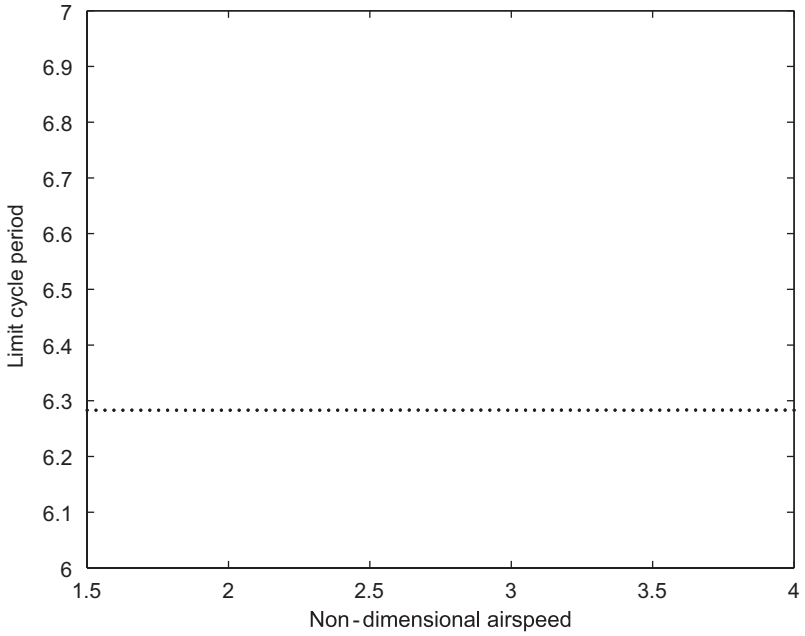

Fig. 5. LCO period using numerical integration for Case 1.

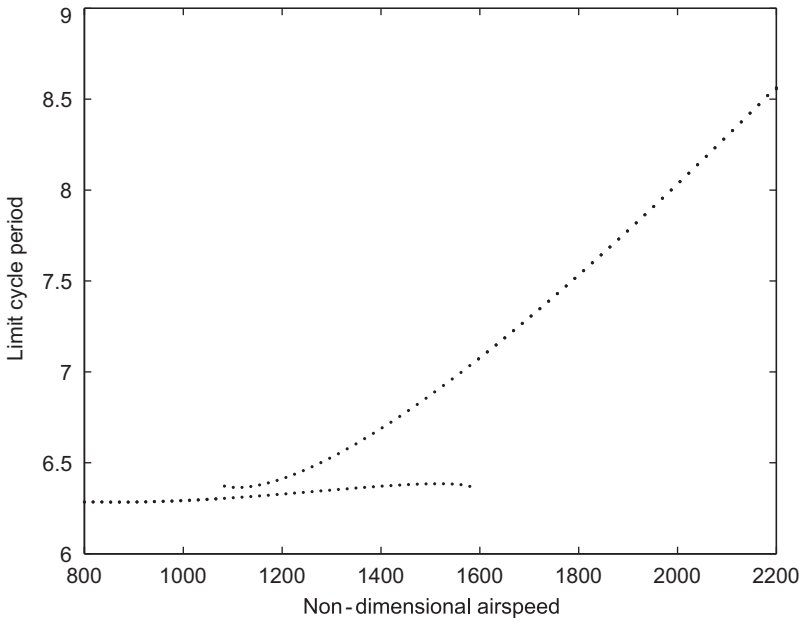

Fig. 6. LCO period using numerical integration for Case 2.

depending on the initial conditions. This indicates the presence of an unstable limit cycle in between these two solutions. At speeds higher than 3.5 there is again only one possible limit cycle.

(ii) *Case* 2: For nondimensional airspeeds lower than $V_c = 864.53$ the response of the system is decaying and the limit cycle amplitude is zero. At speeds between V_c and 1090 the system undergoes LCOs with increasing amplitude. At speeds between 1090 and 1560 two LCO amplitudes exist. At speeds higher than 1560 there is again only one possible limit cycle.

Figs. 5 and 6 show the variation of the LCO period with airspeed, as obtained from numerical integration. For Case 1, the LCO period is constant and always equal to 2π. For Case 2, the period is 2π at low post-bifurcation airspeeds and remains approximately constant while the system responds at the low amplitude LCO. However, the period of the high amplitude LCO increases almost quadratically with airspeed.

It should be mentioned that in order to obtain the plots in Figs. 3 and 4 a large number of very long simulations were carried out. For Case 1 for example, a total of 160 time simulations of 1 million simulation points each were performed. Therefore, even though numerical integration can yield almost the exact behaviour of the system, it can be very time-consuming. The application of the next five methods to the galloping problem is an attempt to speed up the calculation of the bifurcation behaviour of the system without loss of accuracy.

4.2. Cell Mapping

Cell Mapping (Levitas and Weller, 1995) is a stability prediction method for nonlinear systems based on numerical integration. While normal numerical integration consists of a full simulation of the response of a system from some initial conditions, Cell Mapping performs a large number of short integrations from a range of initial conditions, thus mapping the whole parameter space of interest. The system's phase plane is divided into cells and its response is tracked from one cell to another. With this procedure, a complete picture of which cells *map* onto which other cells is built and stability information can be inferred.

The application of Cell Mapping to the galloping problem started by creating cells on the axes of the phase plane, as shown in Fig. 7. The figure shows nine panels on the y-axis and nine panels on the $\dot{y}$-axis, for a total of 18 panels. The panel end-points are denoted by circles and the panel mid-points are denoted by Xs. The panels are numbered consecutively from negative to positive positions, first on the y-axis and then on the $\dot{y}$-axis. Of course, many more panels can be used and they can be linearly spaced or cosinusoidally spaced (such that the panels near the origin are smaller).

The procedure consists of starting simulations using as initial conditions the coordinates of the mid-points of each panel. The simulation stops when the solution has covered 90° on the phase-space. For example, if the simulation is started from a panel on the y-axis, it will stop when it reaches the next time instance where $y = 0$. Similarly, a simulation that begins on the $\dot{y}$-axis will end the next time $\dot{y} = 0$. The mappings of each cell are recorded at the end of each simulation. By following round the destinations of the trajectories starting in each one of the cells it is possible to determine if the system will undergo any limit cycles and what their amplitudes will be. The accuracy of the predicted LCO amplitudes depends on the width of the cells. Decreasing the cell size increases the accuracy but also increases the number of simulations required.

When all the simulations have been performed, a picture of the sort shown in Fig. 8 is obtained. The figure was constructed with 198 linearly spaced cells (cells 1–99 on the y-axis and 100–198 on the $\dot{y}$-axis) for Case 2 of the galloping equation, at a nondimensional airspeed of 1400. In quadrants 1 and 3, there are two areas where the trajectories get closer together (labelled by arrows). These two regions correspond to the two LCOs possible at this airspeed (see Fig. 4). By carefully following all the possible Cell Mappings it can be seen that all the trajectories end up rotating either around cells 6, 185, 94 and 113 (corresponding to an LCO with amplitude in y of 444) or around cells 34, 165, 66, 133 (corresponding to an LCO with amplitude in y of 161.6). The true LCO amplitudes for this airspeed are 443.6 and 159.6. The LCO period can be estimated by adding the simulation times from the first panel in the limit cycle to the last, e.g. the time it takes for the solution to go from panels 6 to 185 plus the time from panels 185 to 94 plus the time from 94 to 133 plus the time from 133 to 34.

This procedure must be repeated at a number of airspeeds in order to build up a full picture of the bifurcation behaviour of the system throughout the airspeed range of interest. A number of parameters must be fine-tuned in order to obtain the best results for each of the airspeeds, including the number and spacing of the panels, the integration time step and the integration stop condition.

4.3. Harmonic Balance

The Harmonic Balance method presented here is based on the formulation of Yang and Zhao (1988) and McIntosh et al. (1981). The main assumption of this technique is that the system follows a sinusoidal limit cycle and, hence, its

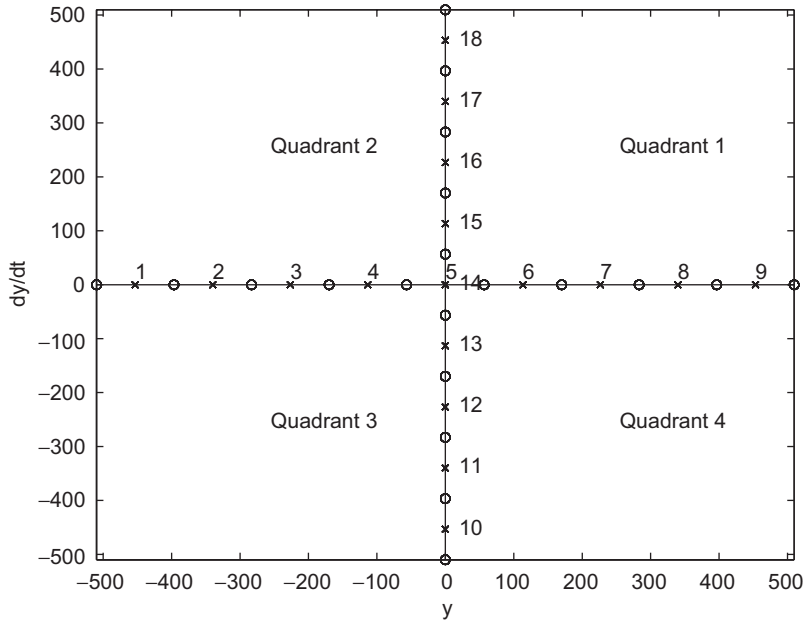

Fig. 7. Subdivision of phase plane axes into cells.

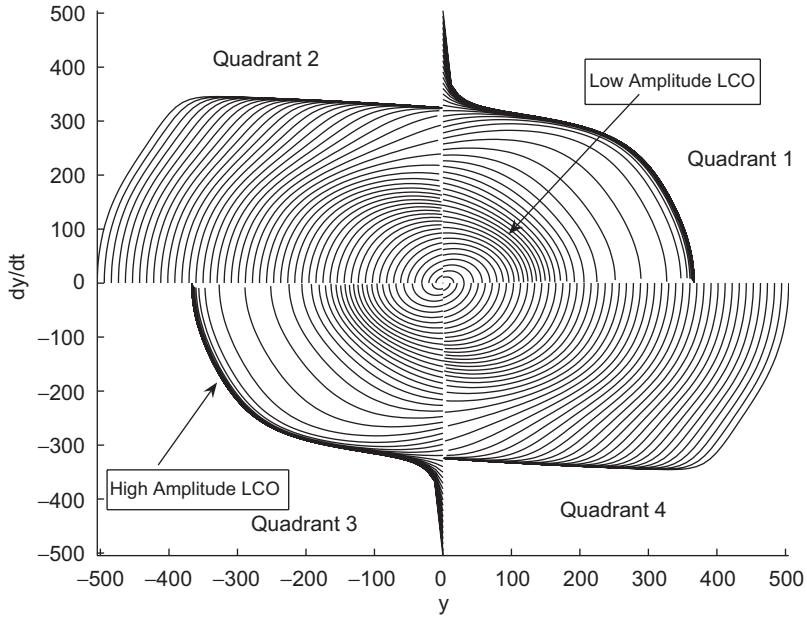

Fig. 8. Phase-plane determined using Cell Mapping. Case 2 and nondimensional airspeed 1400.

response is given by $y = Y\sin(t)$ and $\dot{y} = Y\cos(t)$, where Y is the limit cycle amplitude. Then, using a Fourier series expansion of the nonlinear forces in the system, the nonlinearities are replaced by equivalent linear stiffness and damping terms. For example, consider the equation of motion of a single degree of freedom system:

$$m\ddot{x} + c\dot{x} + kx + f_{nl}(x, \dot{x}) = 0. \tag{7}$$

After applying the Harmonic Balance method, the nonlinear term is replaced by a sum of linear terms:

$$f_{nl}(x,\dot{x}) = K_{\text{eq}}x + C_{\text{eq}}\dot{x}, \tag{8}$$

where K_{eq} and C_{eq} are the equivalent linear stiffness and damping terms, respectively. From Eq. (3) it can be noted that only nonlinear damping is present in the galloping problem, as given in Eq. (5). This nonlinear term can be expanded as a Fourier series, as follows:

$$f(\dot{y}) = \frac{a_0}{2} + \sum_{n=1}^{\infty} a_n \cos(nt) + \sum_{n=1}^{\infty} b_n \sin(nt), \tag{9}$$

where the a_n and b_n coefficients are given by

$$a_0 = \frac{1}{\pi}\int_0^{2\pi} f(\dot{y})\,\mathrm{d}t, \quad a_n = \frac{1}{\pi}\int_0^{2\pi} f(\dot{y})\cos(nt)\,\mathrm{d}t, \quad b_n = \frac{1}{\pi}\int_0^{2\pi} f(\dot{y})\sin(nt)\,\mathrm{d}t. \tag{10}$$

For a first order Harmonic Balance calculation only the first harmonic term is considered, thus only requiring the first term of the Fourier expansion. Assuming that $y = Y\sin(t)$ and $\dot{y} = Y\cos(t)$, the Fourier coefficients become

$$a_0 = \frac{1}{\pi}\int_0^{2\pi} f(Y\cos(t))\,\mathrm{d}t, \quad a_n = \frac{1}{\pi}\int_0^{2\pi} f(Y\cos(t))\cos(t)\,\mathrm{d}t,$$

$$b_n = \frac{1}{\pi}\int_0^{2\pi} f(Y\cos(t))\sin(t)\,\mathrm{d}t. \tag{11}$$

Noting that the nonlinear function is even and that there is no offset, thus giving $a_0 = b_1 = 0$ in the Fourier series expansion, and substituting Eq. (5) into Eq. (11) we have

$$a_1 = \frac{nA}{\pi}\int_0^{2\pi}\left\{\left(V - \frac{2\beta}{nA}\right)Y\cos(t) - \frac{B}{AV}(Y\cos(t))^3 + \frac{C}{AV}(Y\cos(t))^5 - \frac{D}{AV}(Y\cos(t))^7\right\}\cos(t)\,\mathrm{d}t, \tag{12}$$

and after performing the integration the following expression is obtained:

$$a_1 = nA\left(V - \frac{2\beta}{nA}\right)Y - \frac{3nB}{4V}Y^3 + \frac{5nC}{8V^3}Y^5 - \frac{35nD}{64V^5}Y^7. \tag{13}$$

By substituting the Fourier coefficients into Eq. (9) an expression for the equivalent damping coefficient is obtained:

$$C_{\text{eq}} = nA\left(V - \frac{2\beta}{nA}\right) - \frac{3nB}{4V}Y^2 + \frac{5nC}{8V^3}Y^4 - \frac{35nD}{64V^5}Y^6, \tag{14}$$

thus yielding the following equation for the equivalent linearized system:

$$\ddot{y} - \left\{nA\left(V - \frac{2\beta}{nA}\right) - \frac{3nB}{4V}Y^2 + \frac{5nC}{8V^3}Y^4 - \frac{35nD}{64V^5}Y^6\right\}\dot{y} + y = 0. \tag{15}$$

This equation was derived using the assumption that $y = Y\sin t$. Substituting this value yields

$$\left\{nA\left(V - \frac{2\beta}{nA}\right) - \frac{3nB}{4V}Y^2 + \frac{5nC}{8V^3}Y^4 - \frac{35nD}{64V^5}Y^6\right\}Y\cos t = 0, \tag{16}$$

or, for a nontrivial solution (i.e. $Y \neq 0$),

$$nAV^6 - 2\beta V^5 - \frac{3nBV^4}{4}Y^2 + \frac{5nCV^2}{8}Y^4 - \frac{35nD}{64}Y^6 = 0. \tag{17}$$

Eq. (17) can be solved for the amplitudes, Y, of all the possible limit cycles at each given airspeed. The solutions of the equation can be real or complex conjugate pairs. Only the solutions that yield real and positive amplitudes are considered, the others are ignored.

4.4. Higher Order Harmonic Balance

The Harmonic Balance method attempts to approximate the Limit Cycle (or harmonically forced) response of a nonlinear system with a sine wave. The HOHB method (Tamura et al., 1981) extends this concept by making use of sums of sinusoids of various orders, essentially a Fourier series. Consider a general unforced nonlinear system of

the form

$$\dot{\mathbf{x}} = \mathbf{f}(\mathbf{x}, t, \mathbf{p}), \tag{18}$$

where $\mathbf{x}(t)$ is an $m \times 1$ vector of system states, t is the time, $\mathbf{p}$ are system parameters and $\mathbf{f}(\mathbf{x}, t, \mathbf{w})$ is an $m \times 1$ vector of nonlinear functions. Assuming that the system is undergoing LCOs and following the HOHB methodology, the states are approximated by

$$\mathbf{x} = \mathbf{X}_0 + \sum_{k=1}^{N} \mathbf{X}_{k1} \sin k\omega t + \mathbf{X}_{k2} \cos k\omega t, \tag{19}$$

where ω is the fundamental response frequency, $\mathbf{X}_0$, $\mathbf{X}_{k1}$, $\mathbf{X}_{k2}$ are unknown coefficients and N is the order of the approximation. Eq. (19) is substituted into Eq. (18) and then Harmonic Balancing is performed. This consists simply of equating the coefficients of every sine and cosine term to zero. Harmonic balancing leads to $m \times (2N + 1)$ nonlinear algebraic equations in terms of ω, $\mathbf{X}_0$, $\mathbf{X}_{k1}$ and $\mathbf{X}_{k2}$, of the form

$$\mathbf{g}(\mathbf{X}_0, \mathbf{X}_{k1}, \mathbf{X}_{k2}, \omega) = \mathbf{0}, \tag{20}$$

where $\mathbf{g}$ are nonlinear functions. The solution of these equations yields a complete approximation of the true LCO behaviour of the nonlinear system. Notice that there are $m \times (2N + 1) + 1$ unknowns including the frequency and only $m \times (2N + 1)$ equations. This problem can be overcome without loss of generality if, for example, the first element of $\mathbf{X}_{12}$ is set to zero, thus decreasing the number of unknowns to $m \times (2N + 1)$.

There are various different implementations of the HOHB methodology including the HOHB with Newton–Raphson (HOHBNR) (Tamura et al., 1981), the Incremental Harmonic Balance (Lau et al., 1982, 1983) and time domain HOHB schemes such as the Alternating Frequency Time domain approach (Cameron and Griffin, 1989) and the High Dimensional Harmonic Balance (Liu, 2005).

In this work, the HOHBNR approach will be used, in conjunction with the continuation scheme proposed by Leung and Chui (1995). The galloping system's response is written as

$$y = \sum_{k=1}^{N} Y_{k1} \sin k\omega t + Y_{k2} \cos k\omega t, \tag{21}$$

where Y_{k1} and Y_{k2} are unknown coefficients, $Y_{12} = 0$ and k is only allowed to take odd values. The response velocity is the time derivative of Eq. (21), i.e.

$$\dot{y} = \sum_{k=1}^{N} k\omega Y_{k1} \cos k\omega t - k\omega Y_{k2} \sin k\omega t, \tag{22}$$

and the equations of motion are written in first order form as

$$\begin{Bmatrix} \ddot{y} \\ \dot{y} \end{Bmatrix} = \begin{bmatrix} nA\left(V - \dfrac{2\beta}{nA}\right) & -1 \\ 1 & 0 \end{bmatrix} \begin{Bmatrix} \dot{y} \\ y \end{Bmatrix} + \begin{Bmatrix} 1 \\ 0 \end{Bmatrix} nA\left(-\left(\frac{B}{AV}\right)\dot{y}^3 + \left(\frac{C}{AV^3}\right)\dot{y}^5 - \left(\frac{D}{AV^5}\right)\dot{y}^7\right), \tag{23}$$

which is an equation of the form $\dot{\mathbf{z}} = \mathbf{Q}\mathbf{z} + \mathbf{q}f(\mathbf{z})$, where $\mathbf{z} = [\dot{y} \quad y]^{\mathrm{T}}$. The series expansion for $\dot{y}$ is substituted into the nonlinear term and expanded in a Fourier series to yield

$$f(\dot{y}) = f(t) = \sum_{k=1}^{N} F_{k1} \sin k\omega t + F_{k2} \cos k\omega t. \tag{24}$$

The coefficients F_{k1} and F_{k2} can be easily obtained using the Fast Fourier Transform algorithm. Substituting the nonlinear term back into Eq. (24) yields a first order forced linear system of the form

$$\dot{\mathbf{z}} = \mathbf{Q}\mathbf{z} + \mathbf{q}\left(\sum_{k=1}^{N} F_{k1} \sin k\omega t + F_{k2} \cos k\omega t\right), \tag{25}$$

which can easily be solved by substituting

$$\mathbf{z} = \sum_{k=1}^{N} \mathbf{Z}_{k1} \sin k\omega t + \mathbf{Z}_{k2} \cos k\omega t, \tag{26}$$

yielding

$$\begin{Bmatrix} \mathbf{Z}_{k1} \\ \mathbf{Z}_{k2} \end{Bmatrix} = \begin{bmatrix} \mathbf{Q} & -k\omega\mathbf{I} \\ k\omega\mathbf{I} & -\mathbf{Q} \end{bmatrix}^{-1} \begin{Bmatrix} \mathbf{q}F_{k1} \\ \mathbf{q}F_{k2} \end{Bmatrix}. \tag{27}$$

The second element of $\mathbf{z}$, z_2, is equal to y. For a converged solution, $z_2 = y$, or, $Z_{k1_2} = Y_{k1}$ and $Z_{k2_2} = Y_{k2}$. Define a residual $\mathbf{R}_0$ as

$$\mathbf{R}_0 = [Z_{11_2} - Y_{11}, \ldots, Z_{N1_2} - Y_{N1}, Z_{12_2}, \ldots, Z_{N2_2} - Y_{N2}]^{\mathrm{T}}. \tag{28}$$

The object of the HOHB algorithm is to minimize $\mathbf{R}_0$ and can be achieved by means of a Newton–Raphson algorithm. The algorithm's Jacobian can be calculated numerically by increasing each of the Y_{k1}, Y_{k2} (except from Y_{12} which is always zero) and ω by a small amount δY and calculating the new residuals $\mathbf{R}_1$. Then, the corresponding column of the Jacobian is given by $(\mathbf{R}_1 - \mathbf{R}_0)/\delta Y$. Denote the Jacobian by $\mathbf{J}$ and define $\mathbf{Y} = [Y_{11}, \ldots, Y_{N1}, Y_{22}, \ldots, Y_{N2}, \omega]^{\mathrm{T}}$. Then an improved value for $\mathbf{Y}$ is given by $\mathbf{Y} - \Delta\mathbf{Y}$, where $\Delta\mathbf{Y}$ is calculated from

$$\mathbf{J}\Delta\mathbf{Y} = \mathbf{R}_0. \tag{29}$$

The Newton–Raphson procedure is repeated until $\mathbf{R}_0$ is sufficiently small.

Numerous authors have shown that the HOHB method breaks down when applied to a system whose parameter space includes folds. As the galloping problem contains a hysteresis loop resulting from a fold in the bifurcation branch, this issue must be addressed. At the point of inflection, the system Jacobian (and, consequently, the Jacobian of the Newton–Raphson algorithm) becomes singular, causing the HOHB procedure to diverge. One way to overcome this problem is to use the arc-length continuation scheme proposed by Leung and Chui (1995). The Newton–Raphson system is augmented using an additional equation that forces the solution to move in the direction of increasing arc-length along the bifurcation branch. Eq. (29) becomes

$$\begin{bmatrix} \mathbf{J} & \dfrac{\partial \mathbf{R}_0}{\partial V} \\ \dfrac{\partial g}{\partial \mathbf{Y}} & \dfrac{\partial g}{\partial V} \end{bmatrix} \begin{Bmatrix} \Delta\mathbf{Y} \\ \Delta V \end{Bmatrix} = \begin{Bmatrix} \mathbf{R}_0 \\ \Delta\eta \end{Bmatrix}, \tag{30}$$

where η is an arc-length parameter defined as $\eta = g(\mathbf{Y}, V)$ and the function g is chosen as described in Leung and Chui (1995). Assuming that $\mathbf{Y}$ is a converged solution at airspeed V, then Eq. (30) yields a new converged solution at $V - \Delta V$, ensuring that $V - \Delta V$ is in the direction of increasing arc-length parameter η. The increment $\Delta\eta$ must be carefully chosen to ensure convergence.

4.5. Centre Manifold stability

Consider a nonlinear system of the form

$$\dot{\mathbf{x}} = \mathbf{f}(\mathbf{x}, \lambda), \tag{31}$$

where $\mathbf{x}$ are the system states, $\mathbf{f}$ are nonlinear functions and λ is a scalar parameter.

In this paper, a simple linearization approach is introduced, based on the Centre Manifold theorem [see, e.g., Verhulst (1996)]. In this approach, the nonlinear part of the system can be replaced by $\mathbf{f}(\mathbf{x}_0)/\mathbf{x}_0$ such that the equations of motion (31) become

$$\dot{\mathbf{x}} = \frac{\mathbf{f}(\mathbf{x}_0)}{\mathbf{x}_0}\mathbf{x}, \tag{32}$$

where $\mathbf{x}_0$ is a fixed point of the system. Of course, this substitution is only valid in the case where

$$\lim_{\|\mathbf{x}\| \to \|\mathbf{x}_0\|} \frac{\|\mathbf{f}(\mathbf{x})\|}{\|\mathbf{x}\|} = 0, \tag{33}$$

or, in simpler terms, $\lim_{\mathbf{x} \to \mathbf{x}_0} \mathbf{f}(\mathbf{x})/\mathbf{x}$ must be finite. This condition is usually valid for polynomial nonlinearities (Carr, 1981).

Using Eq. (32) the nonlinear system is linearized in the neighbourhood of the fixed point $\mathbf{x}_0$. Due to the Centre Manifold theorem, the stability of the nonlinear system in this neighbourhood is similar to the stability of the linearized system.

Applying this type of linearization to the galloping problem, whose nonlinear function is expressed in Eq. (5), yields the equation

$$\ddot{y} + y = nA\left[\left(V - \frac{2\beta}{nA}\right) - \left(\frac{B}{AV}\right)\dot{y}_0^2 + \left(\frac{C}{AV^3}\right)\dot{y}_0^4 - \left(\frac{D}{AV^5}\right)\dot{y}_0^6\right]\dot{y}. \tag{34}$$

This equation is useful only for determining the primary bifurcation speed. Substituting $\dot{y}_0 = 0$, the damping term becomes $(nAV - 2\beta)\dot{y}$ and, consequently, equal to zero when $V = 2\beta/nA$. However, a much more useful equation can be obtained if the linearization is allowed to continue away from the fixed point, i.e.

$$\ddot{y} + y = nA\left[\left(V - \frac{2\beta}{nA}\right) - \left(\frac{B}{AV}\right)\dot{y}_i^2 + \left(\frac{C}{AV^3}\right)\dot{y}_i^4 - \left(\frac{D}{AV^5}\right)\dot{y}_i^6\right]\dot{y}, \tag{35}$$

where $\dot{y}_i$ is the ith value of $\dot{y}$ at which the linearization is performed. Hence, for a given airspeed V, a number of linearized systems can be constructed for values of $\dot{y} = \dot{y}_1, \dot{y}_2, \ldots, \dot{y}_i$. The stability of each of these i systems can be determined by calculating the eigenvalues $\lambda_1(\dot{y}_i)$ and $\lambda_2(\dot{y}_i)$, using

$$\lambda_{1,2}(\dot{y}_i) = \frac{nA}{2}\left[\left(V - \frac{2\beta}{nA}\right) - \left(\frac{B}{AV}\right)\dot{y}_i^2 + \left(\frac{C}{AV^3}\right)\dot{y}_i^4 - \left(\frac{D}{AV^5}\right)\dot{y}_i^6\right] \pm \frac{1}{2}\sqrt{n^2A^2\left[\left(V - \frac{2\beta}{nA}\right) - \left(\frac{B}{AV}\right)\dot{y}_i^2 + \left(\frac{C}{AV^3}\right)\dot{y}_i^4 - \left(\frac{D}{AV^5}\right)\dot{y}_i^6\right]^2 - 4}.$$

The stability of the systems depends on the real part of the eigenvalues. Hence, the stability condition is

$$\left(V - \frac{2\beta}{nA}\right) - \left(\frac{B}{AV}\right)\dot{y}_i^2 + \left(\frac{C}{AV^3}\right)\dot{y}_i^4 - \left(\frac{D}{AV^5}\right)\dot{y}_i^6 < 0. \tag{36}$$

Since Eq. (36) is a sixth order polynomial it will have 6 roots. In Fig. 9 the real part of the eigenvalues is plotted against $\dot{y}_i$ for $V = 3$. The resulting curve is symmetric around $\dot{y}_i = 0$. It can be seen that there are four stable and three unstable regions. The boundaries between stable and unstable regions (i.e. the zero-crossings of Eq. (36)) are limit cycles and the values of $\dot{y}_i$ at which they occur give the amplitudes of these limit cycles. The following rules apply: (i) transitions from stable to unstable regions are stable limit cycles; (ii) transitions from unstable to stable regions are unstable limit cycles.

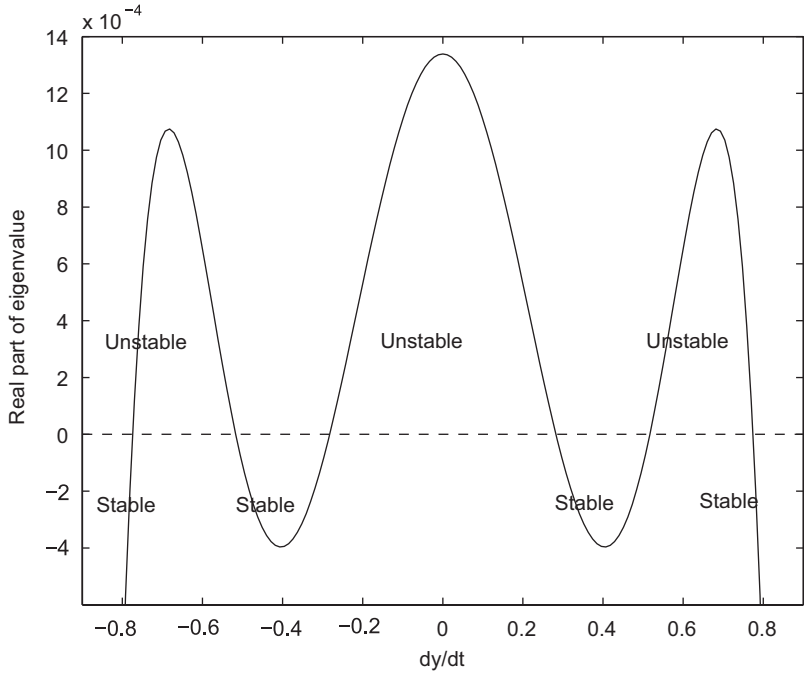

Fig. 9. Variation of real part of eigenvalue with $\dot{y}$ at $V = 3$, Case 1.

According to this analysis, Fig. 9 shows that there are two possible stable limit cycles and one unstable limit cycle at $V = 3$. The analysis can be repeated for different values of V to give a global picture of the stability of the galloping system. In essence, the stability criterion becomes

$$\Re(\lambda_{1,2}(\dot{y}_i, V)) < 0,$$

where $\Re$ denotes the real part.

4.6. Period averaged Normal Form

The classical formulation of the Normal Form theory can be found in many textbooks such as Nayfeh (1993) and Strogatz (1994). Here only the period averaged Normal Form is presented as developed in Leung and Qichang (1998). Before discussing the period averaged Normal Form, a Lie group definition for the Normal Form is required. The Normal Form of an ordinary differential equation satisfies the linearization of a singular vector field

$$ad_j^k F_k^0(y) = 0, \quad k = 2, \ldots, r, \tag{37}$$

where r is the order of approximation of the Normal Form equation, F_k^0 denote the Normal Forms and ad_j^k denote the adjoint operator. The one parameter Lie group Γ is chosen such that the Normal Form is symmetric with respect to Γ, that is

$$F_k^0(\mathrm{e}^{Jt} y) = \mathrm{e}^{Jt} F_k^0(y), \quad \forall t \in R \quad \text{and} \quad \mathrm{e}^{JT} = I, \tag{38}$$

where I is an identity matrix and T is a primitive period.

By applying the classical Normal Form transformation to the autonomous system and the averaging method and Lie group properties to the nonautonomous set of ordinary differential equations, the coordinate transformation is chosen to achieve a transformation from an autonomous into a nonautonomous system by integrating the time variable of the averaged system.

The autonomous equation

$$\dot{x} = Jx + \varepsilon f(x, \varepsilon), \quad x \in \Omega \subset R^n \tag{39}$$

is transformed into the nonautonomous equation

$$\dot{y} = \varepsilon \mathrm{e}^{-Jt} f(\mathrm{e}^{Jt} y, \varepsilon) = \varepsilon g(y, t, \varepsilon) \tag{40}$$

via the following transformation

$$x = \mathrm{e}^{Jt} y, \quad \dot{x} = J\mathrm{e}^{Jt} y + \mathrm{e}^{Jt} \dot{y}. \tag{41}$$

Substitution of Eq. (41) into Eq. (39) yields

$$\mathrm{e}^{Jt} \dot{y} = \varepsilon f(\mathrm{e}^{Jt} y, \varepsilon). \tag{42}$$

and defining

$$g(y, t, \varepsilon) = \mathrm{e}^{-Jt} f(\mathrm{e}^{Jt} y, \varepsilon). \tag{43}$$

Eq. (40) is obtained.

The Normal Form $F_k^0(\zeta)$ of Eq. (40) is obtained by applying the following change of variable:

$$y = \zeta + \sum_{l=1}^{m} \varepsilon h_l(\zeta, t), \tag{44}$$

where the transformation function $h_l(\zeta, t)$ is

$$h_k(\zeta, t) = \frac{1}{T} \int_0^T \tau [g_k(\zeta, \tau + t) - F_k^0(\zeta)] \, \mathrm{d}\tau \tag{45}$$

and

$$g_k(\zeta, t) = \frac{1}{(k-1)!} \frac{\delta^{k-1}}{\delta \varepsilon^{k-1}} g\left(\zeta + \sum_{l=1}^{k-1} \varepsilon^l h_l(\zeta, t), t, \varepsilon \right) \Bigg|_{\varepsilon=0} - \sum_{l=1}^{k-1} h'_{k-l}(\zeta, t) F_l^0(\zeta), \tag{46}$$

in which a prime denotes differentiation with respect to ζ. The period averaged Normal Form is then given by

$$F_k^0(\zeta) = \frac{1}{T}\int_0^T g_k(\zeta,\tau)\,\mathrm{d}\tau. \tag{47}$$

As a result of the averaging process the time variable disappears from Eq. (44) [see Chen and Leung (1998) for proof].

4.6.1. Application to the aeroelastic galloping problem

The equation of motion of the aeroelastic galloping oscillator Eq. (3) can be rewritten in first order form, i.e.

$$\dot{y}_1 = y_2,$$

$$\dot{y}_2 = nA\left[\left(V - \frac{2\beta}{nA}\right)y_2 - \left(\frac{B}{AV}\right)y_2^3 + \left(\frac{C}{AV^3}\right)y_2^5 - \left(\frac{D}{AV^5}\right)y_2^7\right] - y_1. \tag{48}$$

In order to calculate the amplitude of the LCO away from the critical point the airspeed is increased by a small parameter μ

$$V = V_c + \mu. \tag{49}$$

The parameter μ becomes the new bifurcation parameter, working as a speed index, replacing V. By substituting Eqs. (6) and (49) into Eq. (48) and rearranging, we obtain

$$\begin{Bmatrix}\dot{y}_1\\ \dot{y}_2\end{Bmatrix} = \begin{bmatrix}0 & 1\\ -1 & 0\end{bmatrix}\begin{Bmatrix}y_1\\ y_2\end{Bmatrix} + \begin{Bmatrix}0\\ nA\left(\mu y_2 - \left(\frac{B}{AV}\right)y_2^3 + \left(\frac{C}{AV^3}\right)y_2^5 - \left(\frac{D}{AV^5}\right)y_2^7\right)\end{Bmatrix}. \tag{50}$$

The second term on the right-hand side of Eq. (50) contains the nonlinear function and the linear damping, both dependent on the new parameter μ. This term is now ready to be inserted into the Normal Form methodology, by first pre-multiplying the nonlinear function by ε. The final result is a set of two differential equations of the form

$$\dot{r} = f(r), \quad \dot{\theta} = f(r), \tag{51}$$

where r and θ are polar co-ordinates. For an LCO, $\dot{r} = 0$ so that the first equation can be solved for r, representing the LCO amplitude. Substituting the calculation of r into the second equation yields θ, representing the LCO frequency. Note that, r and θ must be transformed back to $(y, \dot{y})$ co-ordinates to obtain the final estimate of LCO amplitude.

4.7. Numerical continuation

Numerical continuation is a highly developed subject, featuring a number of authoritative references, e.g. Allgower and Georg (1990), Kuznetsov (1998) and Beyn et al. (2002). Furthermore, various numerical continuation software tools have been developed and released for general use, such as AUTO (Doedel et al., 1997–2000) and CONTENT (Kuznetsov and Levitin, 1997). Only a brief introduction to the subject is given here.

The main purpose of numerical continuation is to solve an equation of the form $f(\mathbf{x}) = 0$. Numerical continuation allows the computation of a series of points that approximate the desired solution branch. Consider a dynamical system of the form

$$\dot{\mathbf{x}} = f(\mathbf{x}(t), \mathbf{p}) \quad \text{with } f(\mathbf{x}(t), \mathbf{p}) \in R^n, \ \ \mathbf{x}(t) \in R^n, \tag{52}$$

where $f(\mathbf{x}(t), \mathbf{p})$ and $\mathbf{x}(t)$ are real functions and $\mathbf{p}$ is a vector of parameters that affect the stability of the system. The equilibrium states of the system can be calculated by solving the following equation:

$$f(\mathbf{x}(t), \mathbf{p}) = 0. \tag{53}$$

The equilibrium point $x = x_0$ is asymptotically stable at $p = p_0$ if all the eigenvalues of the Jacobian matrix of $f(x_0, p_0)$ have a negative real part. The equilibrium point will be unstable if at least one eigenvalue has positive real part. If a pair of purely imaginary eigenvalues is present the system will undergo a Hopf bifurcation, which gives rise to periodic solutions.

A periodic solution, otherwise known as a limit cycle, describes a close orbit of period T, i.e. $x(0) = x(T)$, in the phase-space plane. When looking for limit cycles the period T is unknown, so an equivalent system is defined in the $[0, 1]$

interval by rescaling the time variable, giving

$$\begin{cases} \mathbf{x}' - Tf(\mathbf{x}(\tau), \mathbf{p}) = 0, \\ x(0) = x(1), \end{cases} \tag{54}$$

where $\tau = t/T$ and $()'$ denotes differentiation with respect to τ. A phase shifted function of the form $\phi(\tau) = x(\tau + s)$ is a solution of Eq. (54) for any value of s. An extra condition is required to obtain a unique solution, which generally takes the form of

$$\int_0^1 \mathbf{x}(\tau)^{\mathrm{T}} \mathbf{x}'_{\mathrm{old}} \mathrm{d}\tau = 0, \tag{55}$$

where $\mathbf{x}'_{\mathrm{old}}$ is the tangent vector of a known limit cycle calculated previously. This condition tries to select the solution with the smallest phase difference with respect to the previous solution $\mathbf{x}'_{\mathrm{old}}$. Eq. (55) has been used as a constraint for this type of problem in Kuznetsov and Levitin (1997) and Doedel et al. (1997–2000).

Stability of bifurcation branches can be determined by using Floquet multipliers. The Floquet multipliers of the periodic solution are obtained by evaluating the eigenvalues of the monodromy matrix of Eq. (52) (Fairgrieve, 1994). A periodic solution always has one multiplier equal to 1. If all the other multipliers are within the unit circle in the complex plane, the solution is stable, otherwise it will be unstable.

4.7.1. Application of MATCONT to the aeroelastic galloping problem

The software package MATCONT (Govaerts et al., 2003) was used to apply numerical continuation to the aeroelastic galloping model to evaluate its effectiveness to predict the limit cycle and hysteretic behaviour of the system. The Floquet multipliers were calculated to confirm the presence of both stable and unstable branches. The model was built using as reference the example in Govaerts et al. (2003). The first equilibrium point was found by specifying a starting velocity in the subcritical region. The equilibrium point, identified as a Hopf point, is then selected and the software is allowed to compute the limit cycle points as the specified parameter, in this case velocity, is increased. When the other two equilibrium points are encountered, the software is commanded to continue the computation until the region of interest has been covered.

5. Results

In this section, the stability predictions from each of the methods will be presented, analysed and compared to numerical integration results. Then, the performances and predictions of the methods will be compared to each other and a judgement will be made as to which are the most accurate and cost-effective methods.

5.1. Cell Mapping results

The LCO amplitude predictions obtained from the Cell Mapping method for Case 1 are plotted in Fig. 10, along with the numerical integration results. It can be seen that Cell Mapping performs very badly. At speeds between the critical speed and 2.3 a range of limit cycles are predicted, all with amplitudes much lower than that of the single true limit cycle. At speeds between 2.3 and 4 the amplitude of the upper branch is predicted with reasonable accuracy but the lower branch is completely missed. Instead, a very wide range of limit cycles is predicted with amplitudes between 0 and 0.4.

The failure of Cell Mapping for Case 1 is due to the very low damping present in the system. Consequently, the system response takes a very long time to subside to the limit cycles. Within the time duration of the short integrations required for Cell Mapping, there is no visible change to the system response, i.e. the system appears undamped and each of the trajectories is seen as a possible limit cycle. In fact, in order to produce Fig. 10 the time of integration was increased significantly. Instead of stopping the integrations when the trajectory has travelled through 90° of the phase-plane, the integrations were stopped after 1260°. Still the quality of the Cell Mapping results are very poor. In order to obtain good quality predictions for all the LCO amplitudes, complete simulations would be needed. Such a procedure, however, would not be Cell Mapping, it would be complete numerical integration. As a result of the failure of the method to predict the correct amplitude, no attempt was made to estimate the LCO period for Case 1 using Cell Mapping.

The galloping system of Case 2 is subject to much higher damping forces and hence settles to its steady-state response far more rapidly. Consequently, Cell Mapping performs very well when applied to this case. Fig. 11 plots the Cell Mapping LCO amplitude predictions and numerical integration results for Case 2. It can be seen that there is very good

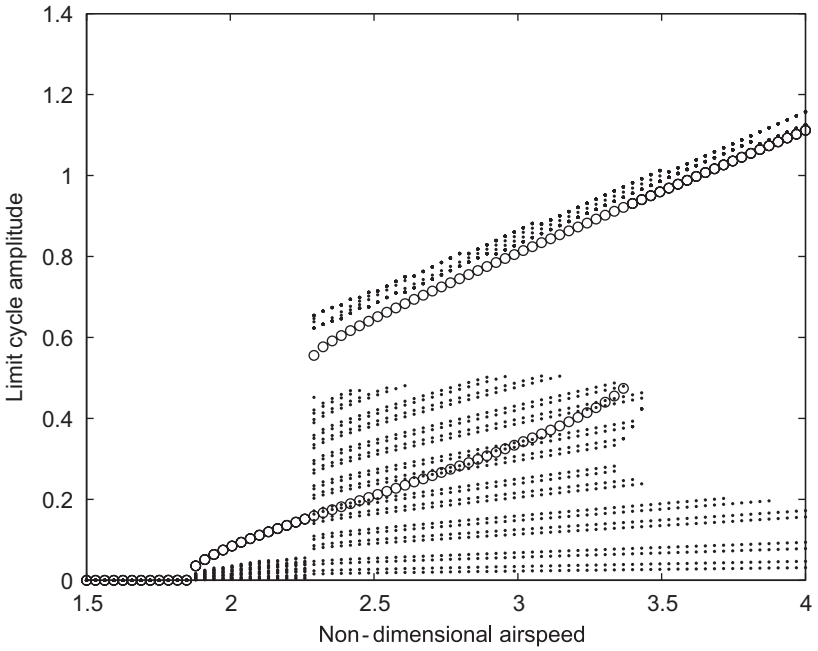

Fig. 10. Comparison between numerical integration (o) and Cell Mapping (.) LCO amplitudes for Case 1.

agreement between the two sets of results. Fig. 12 shows the Cell Mapping estimates of the LCO periods compared to the values obtained from numerical integration. The Cell Mapping periods are always slightly overestimated but, nevertheless, they follow the correct trend. The reason for this overestimation is the fact that the simulations are not stopped when the solution has covered 90° on the phase plane but just afterwards. Therefore, the total error in the estimation of the LCO period can be up to $4\Delta t$.

5.2. Harmonic Balance results

The LCO amplitude predictions obtained from the Harmonic Balance method for Case 1 are plotted in Fig. 13, along with the numerical integration results. The agreement between the two sets of results is almost perfect, indicating that the Harmonic Balance approximation of the galloping equation is satisfactory for LCO amplitudes of the magnitude present in Case 1.

Fig. 14 shows the Harmonic Balance LCO amplitude predictions and numerical integration results for Case 2. In this case the Harmonic Balance method provides very good predictions for the low amplitude part of the bifurcation branch but seriously under-predicts the amplitudes of the LCOs occurring in the high amplitude part. As with most linearization schemes, the Harmonic Balance method is only valid within a region around the system's fixed points. As the response amplitude moves far outside this region, the Harmonic Balance predictions deteriorate. A HOHB scheme is required to increase the size of the region of accurate prediction.

The assumption that $y = Y\sin(t)$ means that the angular frequency of the response is always 1 rad/unit of time. Therefore, the period of all the LCOs predicted for both low and high amplitude cases is 2π. This result is accurate for Case 1, as seen in Fig. 5, but inaccurate for Case 2, as shown in Fig. 6.

5.3. Higher Order Hormonic Balance results

Before the results from the HOHB method are presented it must be stressed that the method is incapable of pinpointing the bifurcation airspeed. If it is applied at subcritical airspeeds then the results will be $Y_{k1} = Y_{k2} = 0$, as the system does not admit periodic solutions. If the continuation algorithm is applied for increasing airspeeds then the solution will remain trivial, even at post-bifurcation airspeeds, since $y = 0$ is a valid solution for the galloping problem at all airspeeds. The only way to obtain nontrivial solutions from the HOHB approach is to apply it post-critically,

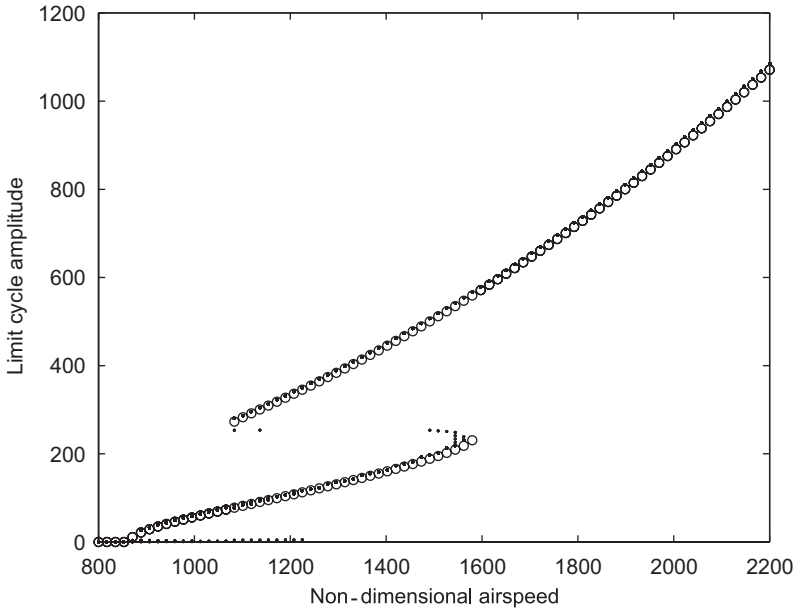

Fig. 11. Comparison between numerical integration (o) and Cell Mapping (.) LCO amplitudes for Case 2.

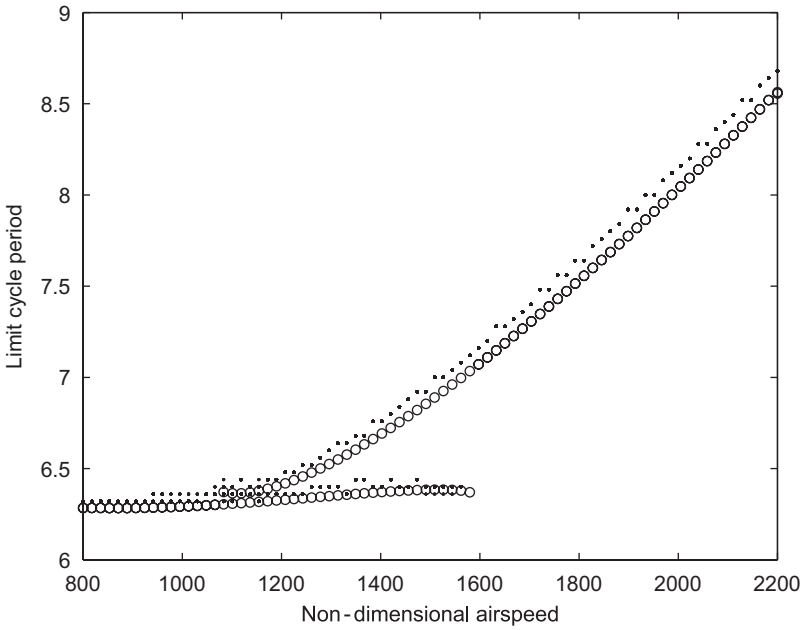

Fig. 12. Comparison between numerical integration (o) and Cell Mapping (.) LCO periods for Case 2.

using the first order Harmonic Balance solution result as an initial guess. Experience shows that only the Y_{11} coefficient and the frequency need to be reasonable guesses, all the other coefficients can be initially set to zero.

The LCO amplitudes predicted by the HOHB method for Case 1 are shown in Fig. 15. A ninth order series was used, although other orders yield identical results. It can be seen that the resulting LCO amplitudes are in perfect agreement with the numerical integration results. The fold is correctly predicted and both stable and unstable LCO amplitudes are calculated. Additionally, the LCO period is equal to 2π, in agreement with the numerical integration results. Notice that

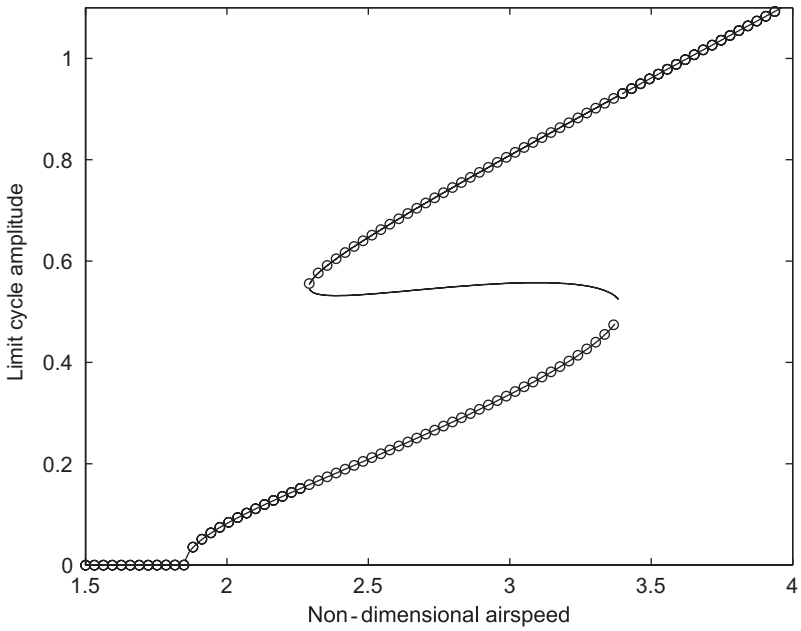

Fig. 13. Comparison between numerical integration (o) and Harmonic Balance (-) LCO amplitudes for Case 1.

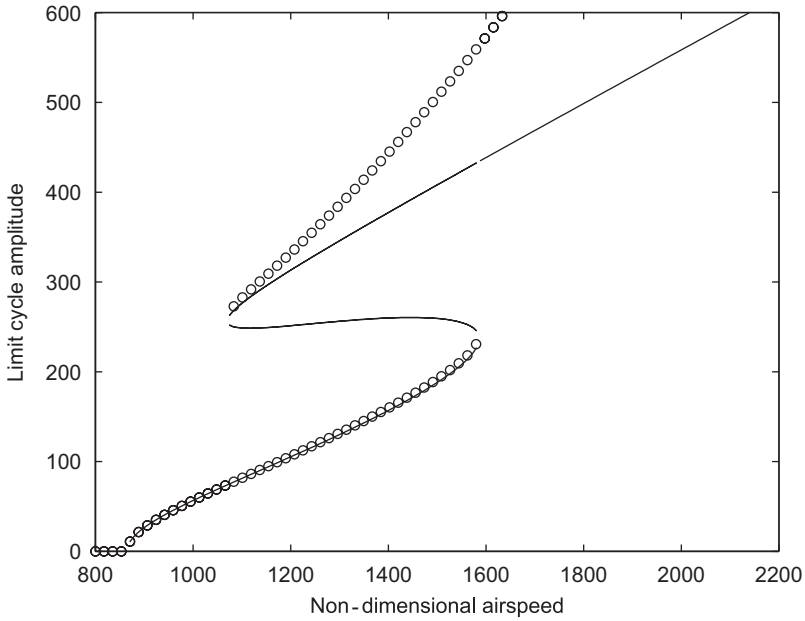

Fig. 14. Comparison between numerical integration (o) and Harmonic Balance (-) LCO amplitudes for Case 2.

there are no results for $V<2$, as the scheme was started at this airspeed. For this case it can be concluded that, although the HOHB approach is accurate, it does not improve on the first order results and, in fact, it requires the latter as a starting point. Therefore, HOHB is not required for Case 1.

Fig. 16 shows the LCO amplitude predictions obtained from the HOHB method for Case 2. Here, a 11th order series was chosen. It can be seen that there is very good agreement between the HOHB and numerical integration results. Only at the highest airspeeds does a slight inaccuracy begin to appear. As with Case 1, the HOHB scheme was

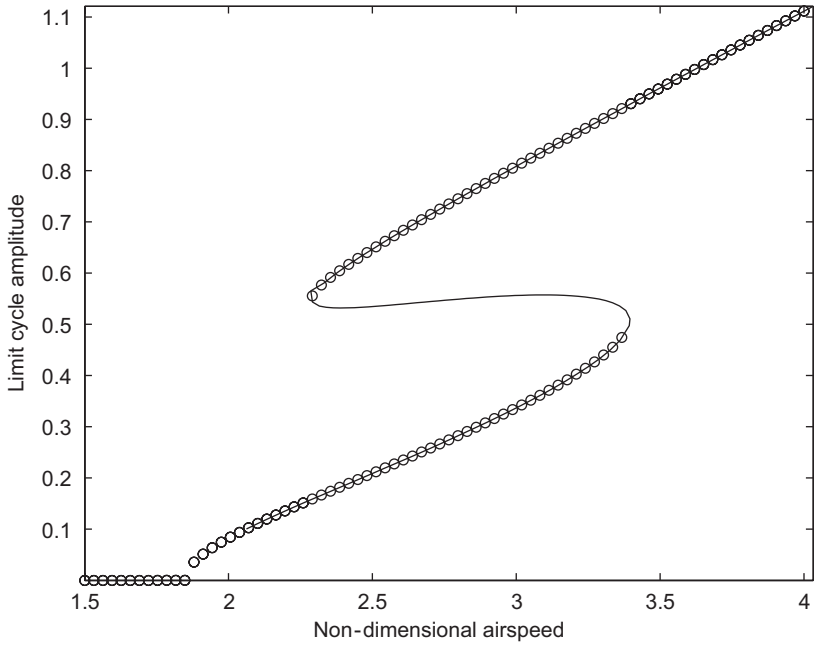

Fig. 15. Comparison between numerical integration (o) and HOHB (-) LCO amplitudes for Case 1.

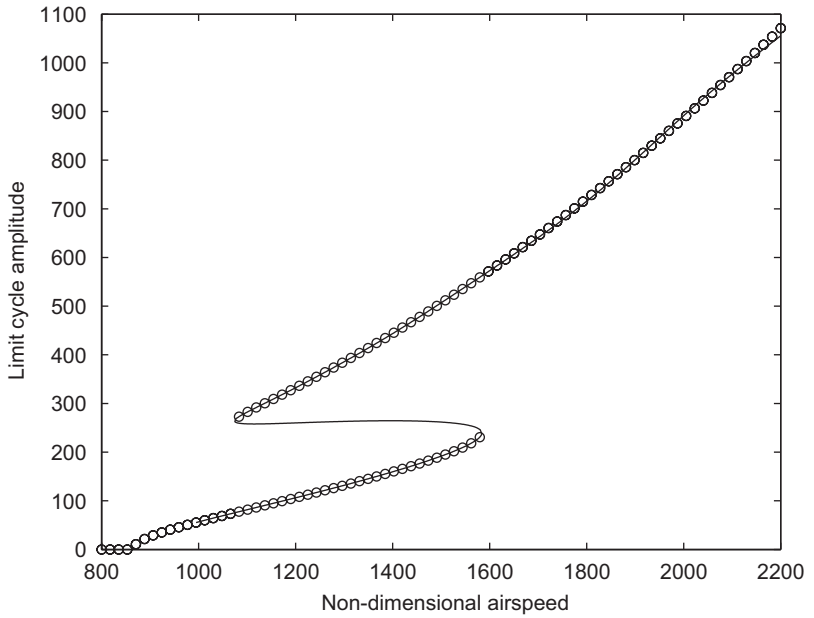

Fig. 16. Comparison between numerical integration (o) and HOHB (-) LCO amplitudes for Case 2.

started post-critically (at $V = 1000$) with the first order result as an initial guess. In this case, though, the accuracy of the HOHB is much higher than that of the first order method. Additionally, the HOHB approach can estimate accurately the LCO period, as shown in Fig. 17 where the HOHB results are compared to numerical integration estimates. Consequently, there are clear advantages to be derived from the application of HOHB to Case 2.

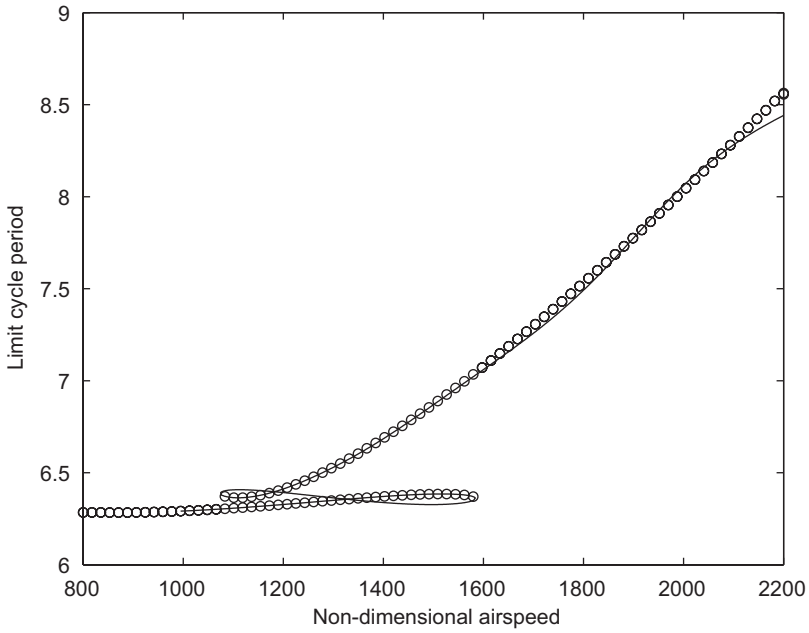

Fig. 17. Comparison between numerical integration (o) and HOHB (-) LCO periods for Case 2.

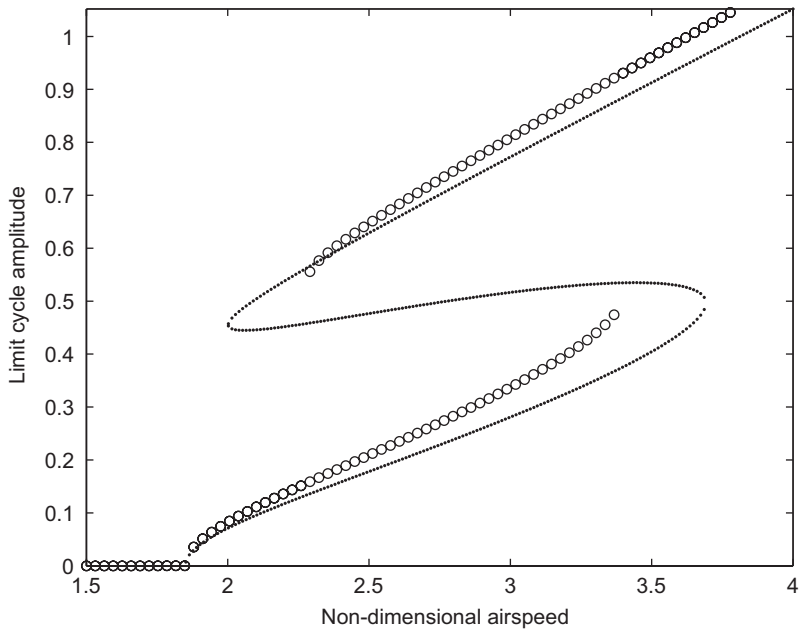

Fig. 18. Comparison between numerical integration (o) and Centre Manifold linearization (.) LCO amplitudes for Case 1.

5.4. Centre Manifold linearization results

The LCO amplitude predictions obtained from the Centre Manifold method for Case 1 are plotted in Fig. 18, along with the numerical integration results. The Centre Manifold predictions for the low amplitude stable LCO are under-predicted from the beginning. The positions of the two turning points are not located very accurately. Finally, the amplitudes of the larger stable LCO are under-predicted throughout.

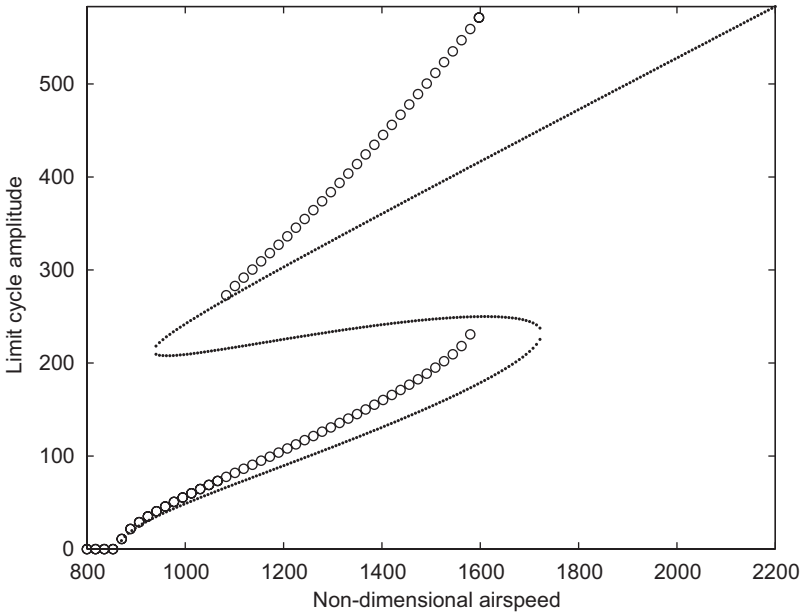

Fig. 19. Comparison between numerical integration (o) and Centre Manifold linearization (.) LCO amplitudes for Case 2.

Fig. 19 shows the Centre Manifold LCO amplitude predictions and numerical integration results for Case 2. In this case, as with the Harmonic Balance method, the Centre Manifold linearization technique seriously under-predicts the Limit Cycle amplitudes for the upper branch. The Centre Manifold approach also under estimates the LCO amplitudes for the lower branch.

As with the Harmonic Balance method, the Centre Manifold Linearization forces the LCO frequency to be always equal to 1 rad/unit of time. Therefore, the LCO period is always 2π for both the high and the low amplitude case. As already discussed, this value is inaccurate for Case 2.

5.5. Normal Form results

For $\beta = 1.07 \times 10^{-3}$ the Normal Form solution obtained is

$$\dot{r} = (V_c + \mu)^{-5}[(-0.3173 - 0.6861\mu - 0.5563\mu^2 - 0.2004\mu^3 - 0.027\mu^4)r^3 + (2.8838 + 3.1175\mu + 0.8425\mu^2)r^5 + 7.0429r^7], \tag{56}$$

$$\dot{\theta} = 0. \tag{57}$$

The steady-state solutions of Eq. (56) for $\mu = 1$ are $r = 0$ and $\pm 0.70344 \pm 0.0946441\mathrm{i}$. The solution corresponding to $r = 0$ determines the unstable origin. The bifurcation behaviour across the velocity range is presented in Fig. 20 for Case 1 and Fig. 21 for Case 2. In both cases there is a degree of agreement with the lower amplitude part of the bifurcation branch but the Normal Form completely misses the higher amplitude and unstable sections. When the value of β is increased to generate a high amplitude limit cycle (Case 2), the solution follows the correct trend for the lower branch but constantly under-predicts the true solution. This difference slowly increases as the solution nears the first turning point. The linearization assumption of the Normal Form seems to break down at these high amplitudes. In both cases the solution never "sees" the upper branch of the bifurcation. Notice that Eq. (57) implies that θ is a constant. In fact, working through the transformations it is determined that the LCO period is always equal to 2π, which is correct for Case 1.

It is of interest to look at the ability of the Normal Form to predict the limit cycle amplitude around the two turning points present within the bifurcation plot. To do this, the equation of motion can be re-written as

$$\begin{Bmatrix} \dot{y}_1 \\ \dot{y}_2 \end{Bmatrix} = \begin{bmatrix} 0 & 1 \\ -1 & 0 \end{bmatrix} \begin{Bmatrix} y_1 \\ y_2 \end{Bmatrix} + \begin{Bmatrix} 0 \\ nA\left(\mu y_2 - \left(\frac{B}{AV}\right)y_2^3 + \left(\frac{C}{AV^3}\right)y_2^5 - \left(\frac{D}{AV^5}\right)y_2^7\right) - k \end{Bmatrix}, \tag{58}$$

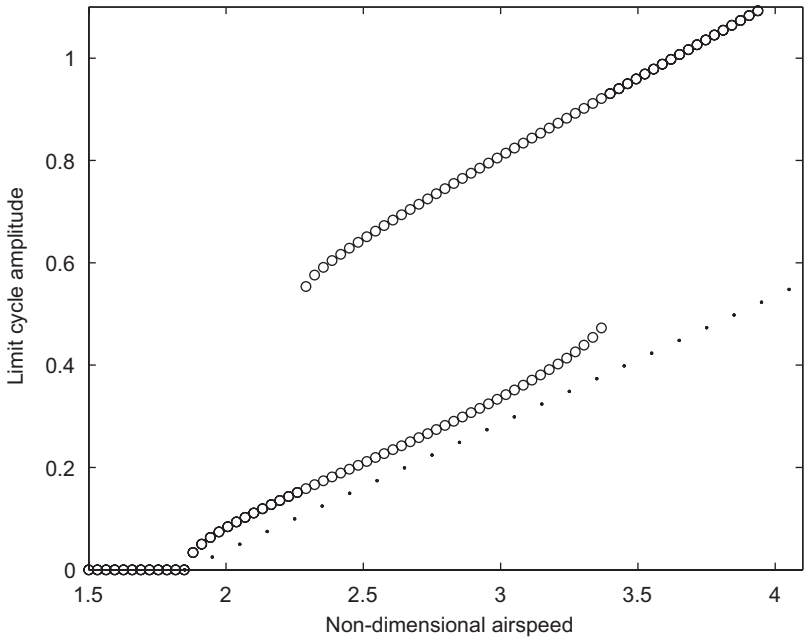

Fig. 20. Comparison between numerical integration (o) and Normal Form (.) LCO amplitudes for Case 1.

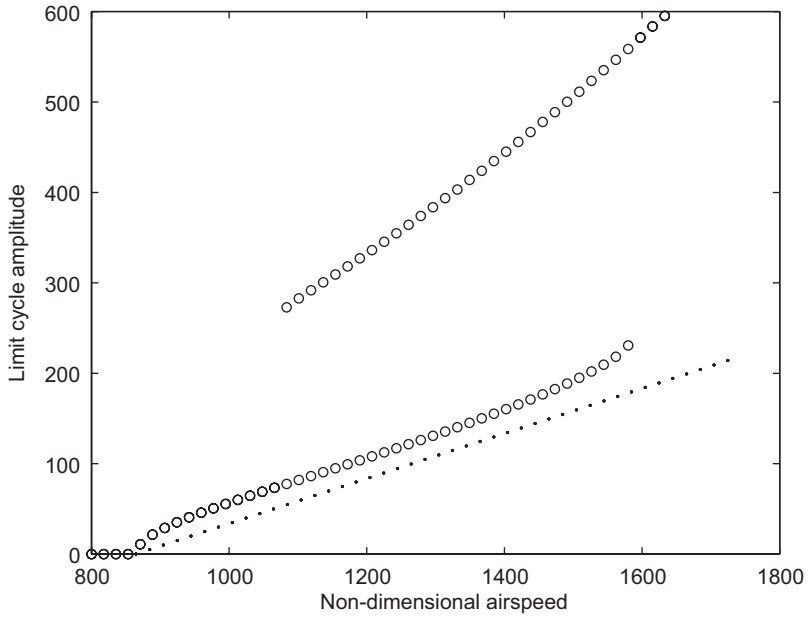

Fig. 21. Comparison between numerical integration (o) and Normal Form (.) LCO amplitudes for Case 2.

Table 1
Location of bifurcation points

	Velocity shift	Amplitude shift
Bifurcation point 1	3.3955	0.5076
Bifurcation point 2	2.2894	0.5486

where a constant term k has been added to allow for the shift in origin of the two new bifurcations. These shifts are tabulated in Table 1for Case 1. They were calculated using numerical continuation.

Fig. 22 shows the result for bifurcation point 1 and Fig. 23 for bifurcation point 2. The star denotes the position of the bifurcation point. In both cases the solution gives excellent agreement with the numerical integration solution. Both

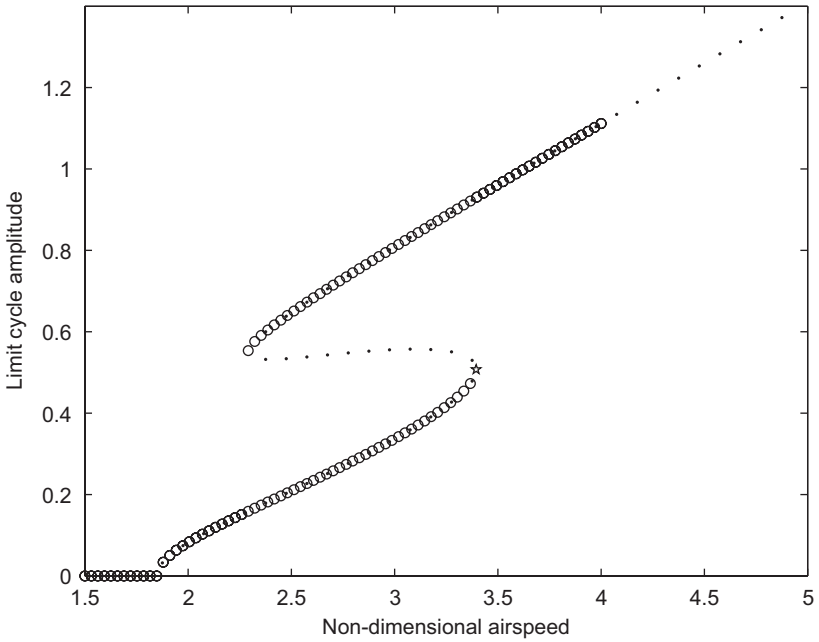

Fig. 22. Comparison between numerical integration (o) and Normal Form (.) LCO amplitudes for Case 1 after moving the origin to the first turning point.

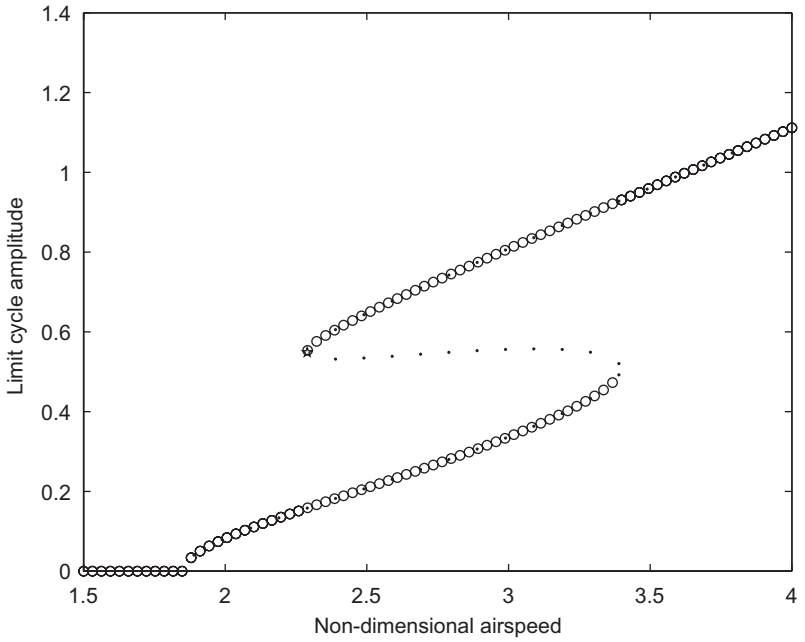

Fig. 23. Comparison between numerical integration (o) and Normal Form (.) LCO amplitudes for Case 1 after moving the origin to the second turning point.

branches are correctly identified, although, as in previous cases, the disagreement between the two curves grows with increasing amplitude. Using these shifts, the Normal Form approach can also predict the position of the unstable limit cycle.

The difference in solution between the turning points and the bifurcation point is due to the manifold curvature. It can be concluded that around the turning points the curvature is very shallow, thus allowing the linearization process to have a much greater radius of convergence.

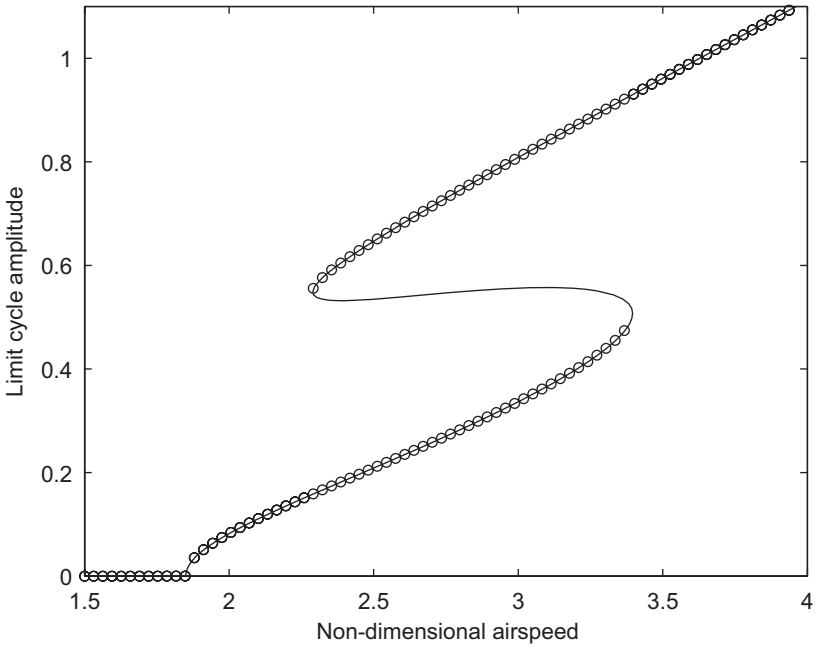

Fig. 24. Comparison between numerical integration (o) and numerical continuation (-) LCO amplitudes for Case 1.

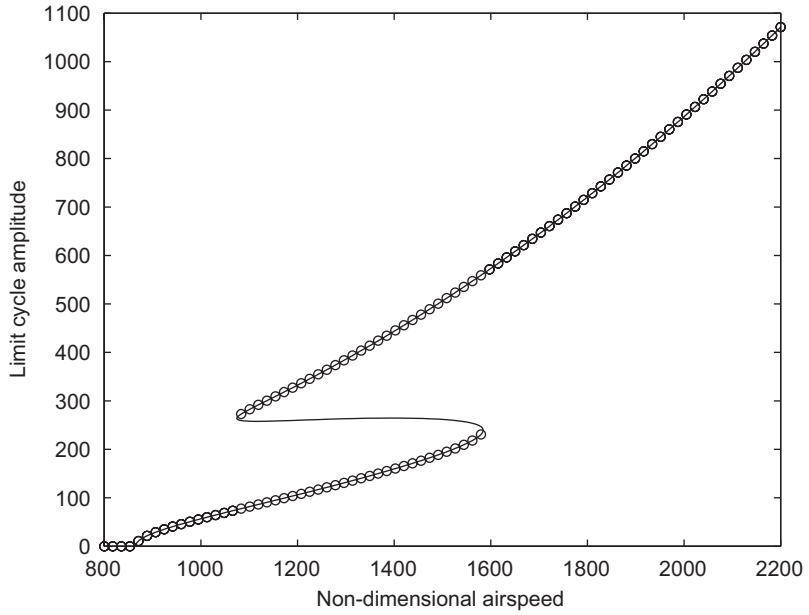

Fig. 25. Comparison between numerical integration (o) and numerical continuation (-) LCO amplitudes for Case 2.

Nevertheless, shifting the Normal Form to the turning points did not improve the bifurcation predictions for Case 2. In fact, no Normal Form could be found around the turning points. Neither amplitude nor period data for the shifted Case 2 are presented.

It should be noted that in order to move the Normal Form solution to one of the two turning points, prior knowledge of the position of these turning points is required. As a consequence, the value of Normal Form as an independent LCO amplitude prediction method is diminished.

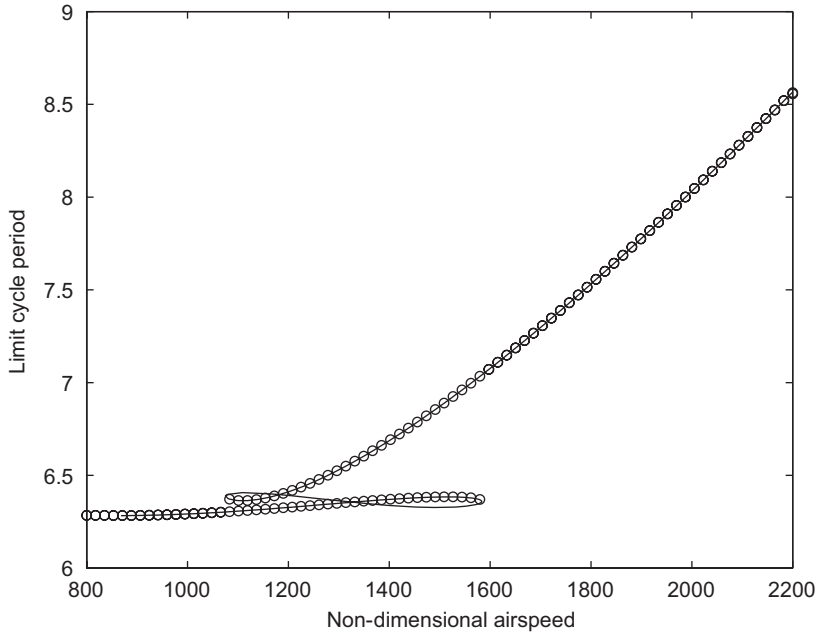

Fig. 26. Comparison between numerical integration (o) and numerical continuation (-) LCO period for Case 2.

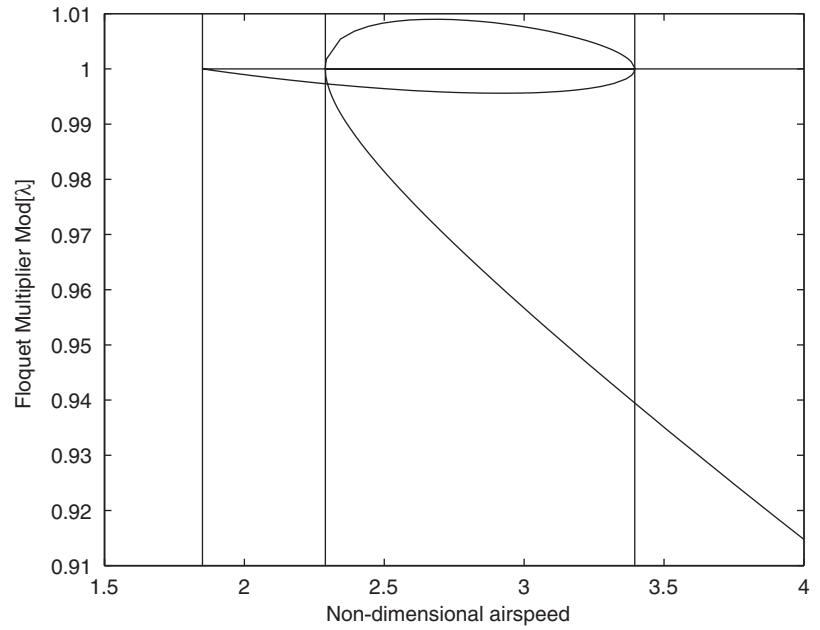

Fig. 27. Floquet multipliers calculated by numerical continuation for Case 1.

5.6. Numerical continuation results

Numerical continuation predicts accurately the LCO amplitude for both Cases 1 (Fig. 24) and 2 (Fig. 25). The turning points are also accurately predicted. The period of the limit cycle for Case 1 does not change throughout the velocity range, remaining constant at a value of 2π. Fig. 26 shows the LCO periods predicted for Case 2 compared to the numerical integration estimates. It is obvious that the agreement is excellent.

The Floquet multipliers are evaluated at various velocities as shown in Fig. 27 for Case 1. Vertical lines are added to show the position of the bifurcation points. As expected, a multiplier is always 1 over the limit cycle range. The other multiplier moves outside the unit circle in the region where two limit cycles co-exist, thus confirming the presence of the unstable section of the solution. The multipliers for Case 2 are presented in Fig. 28.

5.7. Computational performance of methods

In Table 2, the execution times of the computer codes written for all the methods are presented. The calculations were performed on a Powerbook G4 1.25 GHz using Matlab version 7.0.4. The timings of Table 2 are only indicative, as the programming style differed from method to method and all calculations would be faster if they were performed on a more powerful computer. Nevertheless it can be concluded that the Harmonic Balance, Centre Manifold and Normal

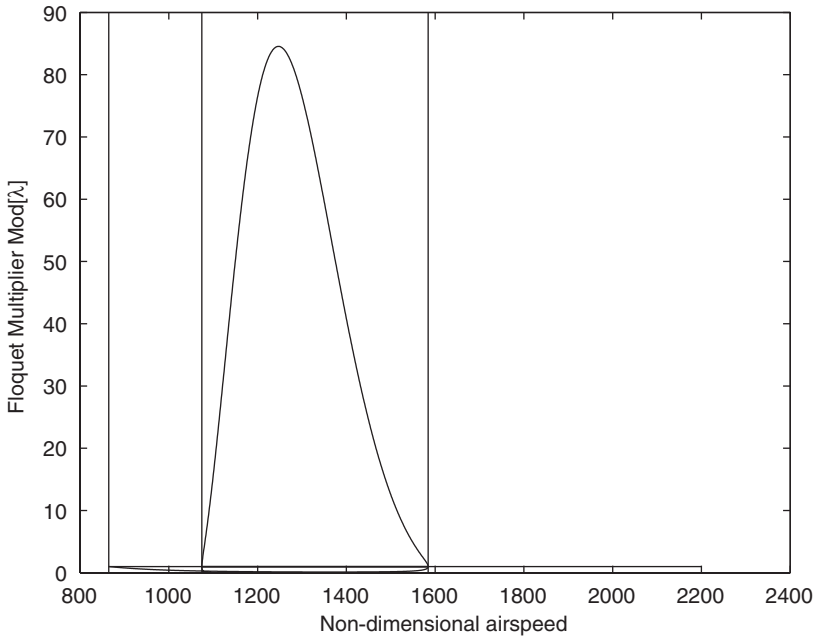

Fig. 28. Floquet multipliers calculated by numerical continuation for Case 2.

Table 2
Execution times

Method	Time Case 1 (s)	Time Case 2 (s)
Numerical integration	4320	1478
Harmonic Balance	0.1	0.1
HOHB	15.1	254.0
Cell Mapping	1303.9	417.3
Centre Manifold	1.0	1.0
Normal Form	0.1	0.1
Numerical continuation	129.9	159.7

Form execution times were the shortest, although these timings do no include execution time from the actual calculation of the equivalent linearized damping and Normal Form expressions, performed using Mathematica.

The HOHB method is significantly slower than the first order Harmonic Balance for both cases. It is faster than numerical continuation for Case 1 but slower for Case 2. Having said that, the speed of both methods depends on various parameters, such as $\Delta\eta$.

It is interesting to note that, even though Cell Mapping was successfully applied to Case 2, the time saving compared to full numerical integration is not substantial. In both cases Cell Mapping execution times were around three times faster which, in the authors' opinion, is not fast enough to justify the use of the method instead of numerical integration, especially since the method fails when applied to systems with low damping.

6. Conclusions

It was found that all the methods, except for HOHB and numerical continuation, performed satisfactorily for only one of the cases. Harmonic Balance and the shifted Normal Form gave very good bifurcation predictions for the low amplitude case but, for the high amplitude case, Harmonic Balance failed to predict accurately one of the limit cycle sections while Normal Form failed completely. Cell Mapping performed very well in the case of the high amplitude galloping problem but failed when applied to the low amplitude case. Additionally, Cell Mapping did not deliver any substantial time savings compared to numerical integration. The simple Centre Manifold approach gave very approximate predictions for both cases.

The HOHB method yielded very accurate predictions for both cases but required a first order Harmonic Balance solution as a starting guess. Numerical continuation predicted accurately both the LCO amplitudes and period, as well as their stability. It should be noted here that a Floquet multiplier calculation algorithm can easily be added the HOHB technique, thus giving it exactly the same capabilities as numerical continuation. The main advantages of numerical continuation is that it can predict the bifurcation point and that it does not require an initial guess.

The HOHB technique could be rendered more efficient if the continuation was performed backwards, i.e. from high to low airspeeds. An initial guess would still be needed but the position of the bifurcation point would not be a problem, as it would be encountered naturally when the airspeed reached the critical value.

The aeroelastic problem studied here has a single degree of freedom and a polynomial nonlinearity, i.e. it is quite simple compared to industrial aeroelastic problems, such as full aircraft in transonic flow. Nevertheless, only two of the methods investigated here managed to fully and accurately characterize the problem, namely numerical continuation and HOHB. This result exemplifies the challenge of nonlinear aeroelasticity.

Acknowledgments

The authors would like to acknowledge the support received by the Engineering and Physical Sciences Research Council and BAE Systems.

References

Allgower, E.L., Georg, K., 1990. Numerical Continuation Methods: An Introduction. Springer, New York.

Attar, P.J., Dowell, E.H., White, J.R., 2005. Modeling delta wing limit-cycle oscillations using a high-fidelity structural model. Journal of Aircraft 42, 1209–1217.

Badcock, K.J., Woodgate, M.A., Richards, B.E., 2005. Direct aeroelastic bifurcation analysis of a symmetric wing based on Euler equations. Journal of Aircraft 42, 731–737.

Bearman, P., Luo, S., 1988. Investigation of the aerodynamic instability by forced oscillation. Journal of Fluids and Structures 2, 161–176.

Bearman, P.W., Luo, S.C., 1987. Experiments on flow induced vibration of a square-section cylinder. Journal of Fluids and Structures 1, 19–34.

Beyn, W.-J., Champneys, A., Doedel, E., Govaerts, W., Kuznetsov, Y.A., Sandstede, B., 2002. Numerical continuation and computation of normal forms. In: Fiedler, B. (Ed.), Handbook of Dynamical Systems, vol. 2. Elsevier, Amsterdam.

Blevins, R.D., 1990. Flow Induced Vibration. Van Nostrand Reinhold, New York.

Cameron, T.M., Griffin, J.H., 1989. An alternating frequency/time domain method for calculating the steady-state response of nonlinear dynamic systems. Journal of Applied Mechanics 56, 149–153.

Carr, J., 1981. Application of Centre Manifold Theory. Springer, Berlin.

Chen, Y., Leung, A.Y.T., 1998. Bifurcation and Chaos in Engineering. Springer, Berlin.

Conner, M.D., Tang, D.M., Dowell, E.H., Virgin, L., 1997. Nonlinear behaviour of a typical airfoil section with control surface freeplay: a numerical and experimental study. Journal of Fluids and Structures 11, 89–109.

Dimitriadis, G., Cooper, J.E., 2000. Characterization of the behaviour of a simple aeroservoelastic system with control nonlinearities. Journal of Fluids and Structures 14, 1173–1193.

Dimitriadis, G., Vio, G., Cooper, J., May 2005. Stability and LCO amplitude prediction for aeroelastic systems with structural and aerodynamic nonlinearities using numerical continuation. In: AVT Symposium on Flow-Induced Unsteady Loads and the Impact on Military Applications. Budapest, Hungary.

Ding, Q., Cooper, J.E., Leung, A.Y.T., 2005. Application of an improved cell mapping method to bilinear stiffness aeroelastic systems. Journal of Fluids and Structures 20, 35–49.

Doedel, E.J., Champneys, A.R., Fairgrieve, T.F., Kuznetsov, Y.A., Sandstede, B., Wang, X.J., 1997–2000. AUTO97-AUTO2000: continuation and bifurcation software for ordinary differential equations (with homcont): user's guide. Technical Report, Concordia University, Montreal, Canada.

Dormand, J.R., Prince, P.J., 1980. A family of embedded Runge–Kutta formulae. Journal of Computational and Applied Mathematics 6, 19–26.

Dowell, E.H. (Ed.), 2004. A Modern Course in Aeroelasticity, fourth ed. Kluwer Academic Publishers, Dordrecht.

Fairgrieve, T.F., 1994. The computation and use of Floquet multipliers for bifurcation. Ph.D. Thesis, University of Toronto, Canada.

Garcia, J.A., 2005. Numerical investigation of nonlinear aeroelastic effects on flexible high-aspect-ratio wings. Journal of Aircraft 42, 1025–1036.

Girodroux-Lavigne, P., Dugeai, A., 2003. Transonic aeroelastic computations using Navier–Stokes equations. In: Proceedings of the CEAS International Forum on Aeroelasticity and Structural Dynamics. Amsterdam, The Netherlands.

Govaerts, W., Dhooge, A., Kuznetsov, Y.A., 2003. MATCONT: a Matlab package for numerical bifurcation of ODES. ACM Transactions on Mathematical Software 29, 141–164.

Hsu, C., 1987. Cell-to-Cell Mapping. Springer, New York.

Kholodar, D.B., Dowell, E.H., Thomas, J.P., Hall, K.C., 2004. Limit-cycle oscillations of a typical airfoil in transonic flow. Journal of Aircraft 41, 1067–1072.

Kim, D.-H., Lee, I., Marzocca, P., Librescu, L., Schober, S., 2005. Nonlinear aeroelastic analysis of an airfoil using CFD-based indicial approach. Journal of Aircraft 42, 1340–1343.

Kuznetsov, Y., Levitin, V., 1997. CONTENT: integrated environment for analysis of dynamical systems. Technical Report, Centrum voor Wiskunde en Informatica, Amsterdam.

Kuznetsov, Y.A., 1998. Elements of Applied Bifurcation Theory. Springer, New York.

Lau, S.L., Cheung, Y.K., Wu, S.Y., 1982. A variable parameter incrementation method for dynamic instability of linear and nonlinear systems. Journal of Applied Mechanics 49, 849–853.

Lau, S.L., Cheung, Y.K., Wu, S.Y., 1983. Incremental Harmonic Balance method with multiple time scales for aperiodic vibration of nonlinear systems. Journal of Applied Mechanics 50, 871–876.

Lee, B.H.K., Liu, L., Chung, K.W., 2005. Airfoil motion in subsonic flow with strong cubic restoring forces. Journal of Sound and Vibration 281, 699–717.

Lee, C.L., 1986. An iterative procedure for nonlinear flutter analysis. AIAA Journal 24, 833–840.

Leung, A.Y.T., Chui, S.K., 1995. Non-linear vibration of coupled Duffing oscillators by an improved incremental harmonic balance method. Journal of Sound and Vibration 181, 619–633.

Leung, A.Y.T., Qichang, Z., 1998. Higher order normal form and period averaging. Journal of Sound and Vibration 217, 795–806.

Levitas, J., Weller, T., 1995. Poincaré linear interpolated cell mapping: method for global analysis of oscillating systems. Journal of Applied Mechanics 62, 489–495.

Liu, L., 2005. Higher order harmonic balance analysis for limit cycle oscillations in an airfoil with cubic restoring forces. In: Proceedings of the 46th AIAA/ASME/ASCE/AHS/ASC Structures, Structural Dynamics and Materials Conference, Austin, Texas, April.

Liu, L., Wong, Y.S., Lee, B.H.K., 1999. Application of the centre manifold theory in non-linear aeroelasticity. Journal of Sound and Vibration 234, 641–659.

Luo, S.C., Chew, Y.T., Ng, Y.T., 2003. Hysteresis phenomenon in the galloping oscillation of a square cylinder. Journal of Fluids and Structures 18, 103–118.

McIntosh Jr., S.C., Reed, R.E., Rodden, W.P., 1981. Experimental and theoretical study of nonlinear flutter. Journal of Aircraft 18, 1057–1063.

Nam, C., Chen, P.C., Liu, D.D., Urnes, R., Yurkovich, R., 2001. Adaptive reconfigurable control of F/A-18 stores limit cycle oscillations. In: Proceedings of the CEAS International Forum on Aeroelasticity and Structural Dynamics, Madrid, Spain, June.

Nayfeh, A.H., 1993. Methods of Normal Forms. Wiley, New York.

Norberg, C., 1993. Flow around rectangular cylinders-pressure and wake frequencies. Journal of Wind Engineering and Industrial Aerodynamics 49, 187–196.

Parkinson, G., 1989. Phenomena and modelling of flow-induced vibrations of bluff bodies. Progress in Aerospace Sciences 26, 169–224.

Parkinson, P., Brooks, N.P.H., 1961. On the aeroelastic instability of bluff cylinders. Journal of Applied Mechanics 28, 252–258.

Parkinson, P., Smith, J.D., 1964. The square prism as an aeroelastic non-linear oscillator. Quarterly Journal of Mathematical and Applied Mathematics 17, 225–239.

Patil, M.J., Hodges, D.H., Cesnik, C.E.S., 2001. Limit cycle oscillations in high-aspect-ratio wings. Journal of Fluids and Structures 15, 107–132.

Price, S.J., Alighanbari, H., Lee, B.H.K., 1995. The aeroelastic behaviour of a two-dimensional airfoil with bilinear and cubic structural nonlinearities. Journal of Fluids and Structures 9, 175–193.

Raghothama, A., Narayanan, S., 1999. Non-linear dynamics of a two-dimensional airfoil by incremental harmonic balance method. Journal of Sound and Vibration 226, 493–517.

Roberts, I., Jones, D.P., Lieven, N.A.J., Bernado, M.D., Champneys, A.R., 2002. Analysis of piecewise linear aeroelastic systems using numerical continuation. Proceedings of the IMechE Part G: Journal of Aerospace Engineering 216, 1–11.

Scruton, C., 1960. The use of wind tunnel in industrial research. Report 309, AGARD.

Simiu, E., Scanlan, R.H., 1996. Wind Effect on Structures: Fundamentals and Applications to Design. Wiley, New York.

Strogatz, S.H., 1994. Nonlinear Dynamics and Chaos: With Applications to Physics, Biology, Chemistry, and Engineering. Perseus Books, Cambridge, MA.

Tamura, H., Tsuda, Y., Sueoka, A., 1981. Higher approximation of steady oscillations in nonlinear systems with single degree of freedom. Bulletin of the JSME 23, 1616–1624.

Thomas, J.P., Dowell, E.H., Hall, K.C., 2004. Modeling viscous transonic limit-cycle oscillation behavior using a harmonic balance approach. Journal of Aircraft 41, 1266–1274.

Verhulst, F., 1996. Nonlinear Differential Equations and Dynamical Systems, second ed. Springer, Berlin.

Vio, G.A., Cooper, J.E., 2005. Limit cycle oscillation prediction for aeroelastic systems with discrete bilinear stiffness. International Journal of Applied Mathematics and Mechanics 3, 100–119.

Woodgate, M.A., Badcock, K.J., Rampurawala, A.M., Richards, B.E., Nardini, D., Henshaw, M.J.deC., 2005. Direct aeroelastic bifurcation analysis of a symmetric wing based on Euler equations. Journal of Aircraft 42, 1005–1012.

Yang, Z.C., Zhao, L.C., 1988. Analysis of limit cycle flutter of an airfoil in incompressible flow. Journal of Sound and Vibration 123, 1–13.